Construction and Building Materials 318 (2022) 125992

Contents lists available at ScienceDirect

Construction and Building Materials

journal homepage: www.elsevier.com/locate/conbuildmat

Role of inclusion size distribution of titanium dioxide on the nitrogen oxides reduction capability and microstructural characteristics of cementitious systems

Emrah Bahşi [a], Oğuzhan Şahin [b], Hüseyin İlcan [a,c], Burak Uzal [d], Muhammed Faruk Günal [c], Gürkan Yıldırım [c], Mustafa Şahmaran [c,*]

[a] Institute of Science, Hacettepe University, Ankara, Turkey
[b] Department of Civil Engineering, Kırşehir Ahi Evran University, Kırşehir, Turkey
[c] Department of Civil Engineering, Hacettepe University, Ankara, Turkey
[d] Department of Civil Engineering, Abdullah Gül University, Kayseri, Turkey

ARTICLE INFO

Keywords:
Titanium dioxide (TiO_2)
Photocatalytic activity
Cementitious systems
Nitrogen oxides (NO_x) degradation
Inclusion size distribution
Hydration

ABSTRACT

This paper explores the effect of the inclusion size of titanium dioxide (TiO_2) particles on a variety of performance properties of cementitious systems via experimental studies. In addition to comprehensive microstructural analysis including pore size distribution and scanning electron microscopy with energy-dispersive X-ray spectroscopy (SEM-EDX) analyses, particular consideration was given to the effect of particle size distribution (PSD) of TiO_2 particles on mechanical and photocatalytic properties and hydration kinetics of cementitious systems. Nano-sized, submicron-sized and micron-sized anatase-phase TiO_2 powders were utilized as photocatalysts at a dosage of 5% by total weight of powder material. In addition to the single use of TiO_2 particles with three different size ranges (nano, submicron and micron), they were also used in combination by adjusting their PSDs with three different PSD moduli (q): 0.1, 0.5, and 0.9. Test results show that techniques for achieving optimal microstructural characteristics of cementitious systems also help design and improve their performance in favor of multifunctionality. As a result of PSD optimization of TiO_2 particles with three different size ranges, which was significantly influential on the microstructure of the cementitious systems, superior photocatalytic degradation results were obtained from mixtures containing lower amounts of nano-sized TiO_2 particles. Cementitious composites with denser microstructure showed lower performance in terms of being able to maintain photocatalytic degradation capability for a prolonged period, whereas the opposite was the case for compressive strength.

1. Introduction

Air pollution has become a major global issue with negative environmental, economic and health impacts. To overcome this problem, many approaches have been taken to eliminate or reduce polluting emissions such as carbon monoxide, sulfur oxides and nitrogen oxides (NO_x) sustained in air [1–8]. Nitrogen oxide (NO_x [NO and NO_2]) leads to the formation of ozone gases and acid rain [9–10], and is particularly detrimental to the health of living things. To reduce its negative effects, it should be captured and permanently stored as harmless substances, using efficient process facilities/methods. In that regard, multifunctional advanced materials with NO_x reduction capability have been gaining importance with sectors looking to improve air quality: the construction industry is one of those sectors. Their focus is shifting towards use of NO_x-reducing materials (photocatalysts) in cementitious systems to provide air purifying properties and decrease environmental burden. In this regard, materials such as titanium dioxide (TiO_2), zinc oxide (ZnO) and cadmium oxide (CdO) are photocatalysts frequently used by the construction sector worldwide [11–12]. Among all the available materials capable of reducing NO_x under ultraviolet (UV) radiation, TiO_2 is recommended for use in cementitious systems due to its cost-effectiveness, high photocatalytic degradation capability [13], chemical stability, non-toxicity in the cement matrix and remaining in an inert state unless exposed to UV radiation [12,14–15].

* Corresponding author at: Department of Civil Engineering, Hacettepe University, Ankara, Turkey.
E-mail address: sahmaran@hacettepe.edu.tr (M. Şahmaran).

https://doi.org/10.1016/j.conbuildmat.2021.125992
Received 4 September 2021; Received in revised form 9 November 2021; Accepted 1 December 2021
Available online 10 December 2021

Photocatalytic degradation capability of the TiO_2-incorporated cementitious systems is directly related to the surface morphology, specific surface area and particle size of TiO_2 utilized and the number of photocatalyst particles on UV-reached surfaces of photocatalytic cementitious systems. Considering that the particle size of TiO_2 is a significantly influential factor on the activity of photocatalytic systems, studies addressing the relationship between the particle size of TiO_2 incorporated into the cement-based systems and photocatalytic activity of such systems have been performed. Seo and Yun [16] used 35 nm- and 100 nm-sized TiO_2 particles, and obtained higher NO removal rate from mortar mixtures produced with smaller TiO_2 particles (35 nm) compared to those with larger ones (100 nm). Their results were found attributable to the fact that (i) smaller-size particles mean the presence of larger number of particles and thereby large surface area beneficial for NO absorption capability, and (ii) smaller-size particles provide higher amount of active surface areas. Similarly, Chen and Poon [17], Husken et al., [18]; Hunger et al., [19], Meng et al., [20] and Folli et al., [21] found results indicating that TiO_2 particles with higher surface area exhibits better photocatalytic degradation capability compared to TiO_2 with lower surface area. Although high photocatalytic efficiency of nano-sized TiO_2 particles compared to larger-sized TiO_2 particles [22–27], considering the fact that obtaining nano-sized particles requires a costly, demanding and intense production process, to ensure more sustainable and cost-effective air cleaning through photocatalytic reactions stimulated in TiO_2-incorporated cementitious systems, cheaper larger-sized TiO_2 particles should be included in the photocatalytic cement-based systems along with nano-sized ones to improve performances of cementitious systems other than photocatalytic performance in favor of multifunctionality. Although the properties of TiO_2 used as photocatalyst in cement-based systems have significant effects on the NO_x degradation capability, the microstructure of such systems (the number of voids and pores and pore size distribution) undeniably affects the activity as well. Pérez-Nicolás et al. [28] manufactured mortars with different types of binders namely, Portland cement, high-alumina cement, low-alumina cement and dry slaked lime and obtained relatively higher photocatalytic degradation activity from mortars prepared by using high-alumina cement and lime separately, which contained higher amounts of pores with diameters above 0.05 μm allowing easier reach of NO molecules into the more in-depth parts of the mortars in favour of further contact between the surface of photocatalytic materials and pollutants. Lucas et al. [29] prepared several mortars by using different types of binders (e.g. lime, cement and gypsum) and established links between the microstructure and photocatalytic performance of these mortars. They emphasized that high porosity promotes the photocatalytic activity through facilitating the gas diffusion in an effort to assist the contact between the photocatalyst and NO_x gas at the irradiated surface, and the diameter of pores should not be less than 1 μm (nanopores) to restrict the gas diffusion, as also reported by Giosuè et al. [30]. Similarly, Sugranez et al. [31] stated that the formation of higher amount of hydration products provides a denser microstructure through the filling of the pores, while lower amount of hydration products and the amount of adsorbed water filling the space between the cement grains provide a more porous structure, which is beneficial for higher photocatalytic activity. They also concluded that photocatalytic activity is enhanced as the total porosity increases due to higher possibility of having larger number of active sites accessible to the molecules needed for the photocatalytic reactions and increasing in the generation/amount of hydroxyl radicals to react with NO_x, and they proposed that poor packaging of aggregate particles [through modification of particle size distribution (PSD)] is a method that can be used to create a macro-porosity structure. In order to achieve improved photocatalytic activity through altering the porosity of cementitious materials, Chen and Poon [17,32] and Poon and Cheung [33] recommended changing the PSD of aggregates or decreasing the cement content of the mixtures. Meng et al. [20], Matěj ka et al. [34], Lee et al. [35], Guo et al. [36], Xu et al. [37–38] and Boonen and Beeldens [39] observed increments in the NO removal rate with increased porosity as well. Chen et al. [40] also noted the positive contribution of porosity to the photocatalytic activity, as it provides a channel for pollutants to easily flow through, more surface area for the deposition of photocatalysts and more space for holding/accumulation of final products, which prevents the covering of the surface of the photocatalyst. Jin et al. [41] stated that the presence of larger amount of micropores (less than 5 nm) in cement-based mortars is beneficial for NO_x uptake.

In the case of co-utilization of TiO_2 particles of different sizes, optimizing PSD of all TiO_2 particles can be essential for optimum performance and/or improvement in performance of systems in several ways. Feret [42] first studied the PSD to obtain more economical concrete mixture designs by filling in voids among particles. The Fuller and Thompson method has also been used for a long time in determining the extent to which concrete aggregates should be mixed during PSD optimization [43]. In 1980, the "minimum particle diameter" technique, which considers the size of the smallest grain used as well as the largest one, was used by Funk et al. [44] to create mixtures with the highest packing density. There have also been other methods used to ensure high compactness of aggregates [45–46]. On the other hand, in addition to PSD optimization of aggregates, proper gradation of powdery materials such as cement or mineral admixtures can fill entire voids among different particles. There are number of studies related to the effects of optimizing the PSD of some powder materials on several properties of cementitious systems. Sevim and Demir [47] studied the effect of optimizing the PSD of fly ash on the performance of cement-based systems in terms of mechanical and durability perspectives. They concluded that optimizing the PSD of fly ash particles in a proper manner provided much better performance for cementitious systems. Another study of Sevim and Demir [48] investigated changes in physical and permeability properties of cementitious mortars through optimizing the PSD of fly ash. They found that modifying the PSD of fly ash particles as a pozzolanic material has an undeniable effect on the properties of cement-based systems, due to proper PSD playing a major role in filler effect and providing a good distribution of solid concentration. Lim et al. [49] also studied the effects of particle grading on autogenous shrinkage and strength of ultra-high-performance concrete, and they reported that PSD is reasonably influential on these concrete properties.

As results of several literature studies show, the PSD of powder materials has a significant influence on several properties of cementitious systems. However, until now, there have been no specific studies on using different-sized TiO_2 materials with optimized PSD in cementitious systems to improve microstructures in favor of optimum photocatalytic efficiency. In this instance, optimization of the PSD of TiO_2 particles in a wide range of sizes (inert ingredients that can be considered filling materials along with their photocatalytic efficiency) is necessary to improve the engineering properties of cementitious systems and/or the degree of photocatalytic reactions in favor of NO_x degradation capability. Therefore, due to the absence of relevant studies, the authors set out to investigate the effects of PSD of TiO_2 with ternary use of nano-sized, submicron-sized and micron-sized TiO_2 particles on photocatalytic performance and mechanical properties of cementitious systems. The effects of PSD optimization on mechanical properties (compressive strength), physical properties (pore volume and pore size distribution), hydration kinetics and NO_x degradation capability were investigated using different distribution modules. In addition, microstructural features of specimens were examined by microstructural characterization analyses including scanning electron microscopy with energy-dispersive X-ray spectroscopy (SEM/EDX).

2. Experimental program

2.1. Materials

Considering its lower light absorption ability compared to that of Ordinary Portland Cement (OPC), CEM I 52.5R type White Portland

Cement (WPC) conforming to the EN 197–1 cement standard was used as the main binder material in all mixtures. Its chemical composition and physical properties are summarized in Table 1. Nano-sized, submicron-sized and micron-sized anatase-phase (NA, SMA and MA) TiO_2 powders were used as photocatalysts to degrade the NO in the presence of UV light. Physical properties of different sizes of anatase-phase TiO_2 powders used in this study are presented in Table 2. Different-sized TiO_2 used as photocatalyst material in this study was characterized by using scanning electron microscope (SEM) (Tescan GAIA 3 FIB-SEM operated at 3.0 kV) and X-Ray diffraction measurement (XRD) (Rigaku Ultima-IV diffractometer at 40 kV, within a scan range of $2\theta = 5–80^\circ$ and 30 mA with Cu-Kα ($\lambda = 1.5405$Å) radiation.). To prevent any error in results, a representative sample of powder was obtained from the inside of the premixed powder batch of TiO_2 powders and was dried overnight in an oven before analyzes. X-ray diffraction (XRD) patterns of NA, SMA and MA TiO_2 powders are shown in Fig. 1. The morphology and microstructure of NA, SMA and MA TiO_2 powders obtained by SEM for each size of TiO_2 are presented in Fig. 2.

Two different surfactants were used in this experimental study, namely polycarboxylic ether-based superplasticizer (PCE) and polyphosphates and aminocarboxylate-based liquid polyacrylic acid (PAA). The PCE was liquid, conforming with ASTM-C494/C494M standard [50], with 40% solid material content and a specific gravity of 1.1. The PAA was used to provide particle surface charges with its polyelectrolyte dispersant ability [51]. White, milky liquid PAA contained 48% solid material, with a density of 1.22 kg/l and pH value of in the range of 3–4.5.

2.2. Mixture proportions

All mixtures were prepared at a constant water to powder ratio of 0.35, by weight. Preliminary studies were performed for determining optimum TiO_2 content to be utilized in this study. Specimens prepared with different TiO_2 contents, ranging from 1% to 20% of total weight of powder material, were subjected to NO degradation tests and there was not significant increase in NO removal rate beyond TiO_2 utilization rate of 5% and even declines after a certain point. Therefore, utilization rate of TiO_2 powders was kept constant at 5% of total weight of powder material for all mixtures. NA, SMA and MA TiO_2 powders were used as ternary and their incorporation rates were determined in accordance with the PSD equation proposed by Funk et al. [24]. Various PSD moduli (0.1, 0.5, 0.9) representative of a wide region were used. NA, SMA and MA TiO_2 powders were also used solely. To ensure homogeneous distribution of TiO_2 particles throughout matrix without compromising any other properties of the mixtures, the proper amounts of PCE (around 0.5% of the total weight of powder materials) and PAA (0.5% of total weight) were used as binary surfactant materials in all mixtures. These utilization rates for surfactant materials were chosen based on a previously conducted study by the authors [51].

2.2.1. Particle size distribution of TiO_2 particles

To study the influence of optimizing the PSD of TiO_2 particles in co-utilization of different-sized TiO_2 particles on the mechanical properties and photocatalytic efficiency of the cementitious systems, PSD Equation (1) proposed by Funk et al. [44], was adapted to this study. When using this equation to calculate incorporation rates of TiO_2 powders with different particle size fractions, three sieve diameters of 50 nm, 255 nm and 1110 nm were considered: the maximum grain sizes of each TiO_2 powder batch classified by particle size (NA, SMA, MA; respectively) and the limit values separating the TiO_2 materials from each other in accordance with particle size.

$$P(D) = \frac{D^q - D^q_{min}}{D^q_{max} - D^q_{min}}, \quad (1)$$

where P(D) is the passing percentage of TiO_2 particles passing through relevant sieve, D is the diameter of relevant sieve opening, D_{min} is the minimum particle diameter in all TiO_2 powders and D_{max} is the maximum, and q is the PSD modulus. Three different PSD moduli of 0.1, 0.5 and 0.9 were used. It should be noted that mixtures containing relatively higher proportion of particles with larger grain size were obtained when the numerical value of the PSD modulus increased. NA, SMA and MA TiO_2 powders were also used solely to observe their individual influences on the performance of cementitious systems. In addition, a reference mixture was manufactured without TiO_2 powder content for comparison. PSD curves were plotted using the equation above for values of q: 0.1, q: 0.5 and q: 0.9. These PSD curves and those of NA, SMA and MA TiO_2 powders are displayed in Fig. 3. A total of 7 different mixtures were manufactured: their proportions can be seen in Table 3.

Mixtures are denominated with letters and numbers based on ingredients used in production. M0 is the reference mixture. The second, third and fourth mixtures (MNA, MSMA, MMA) were prepared using TiO_2 powders solely according to their particle size. For example, MNA was prepared using only NA TiO_2 powder. The fifth, sixth and seventh mixtures (MQ0.1, MQ0.5, MQ0.9) were prepared by ternary use of NA, SMA and MA TiO_2 powders with different PSD moduli. For example, MQ0.1 was prepared using a PSD modulus of $q = 0.1$.

Table 2
Physical properties of different sized anatase-phase TiO_2 powders.

Physical Properties	Nano-sized Anatase (NA)	Submicron-sized Anatase (SMA)	Micron-sized Anatase (MA)
Purity (%)	99.86	99.89	99.87
Density (g/cm^3)	3.55	3.55	3.60
Maximum Grain Size (nm)	50	255	1110
Minimum Grain Size (nm)	0.4	50	255

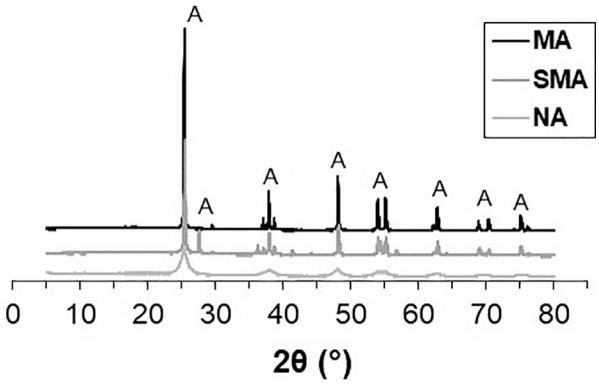

Fig. 1. XRD analysis of MA, SMA and NA TiO_2 (Anatase: A).

Table 1
Chemical composition and physical properties of CEM I 52.5 R WPC.

Chemical Composition, %						Physical Properties		
SiO_2	Al_2O	Fe_2O_3	CaO	MgO	SO_3	Loss on ignition	Density (g/cm^3)	Specific surface, Blaine (cm^2/g)
21.39	3.37	0.89	62.6	2.39	4.55	3.1	3.15	4650

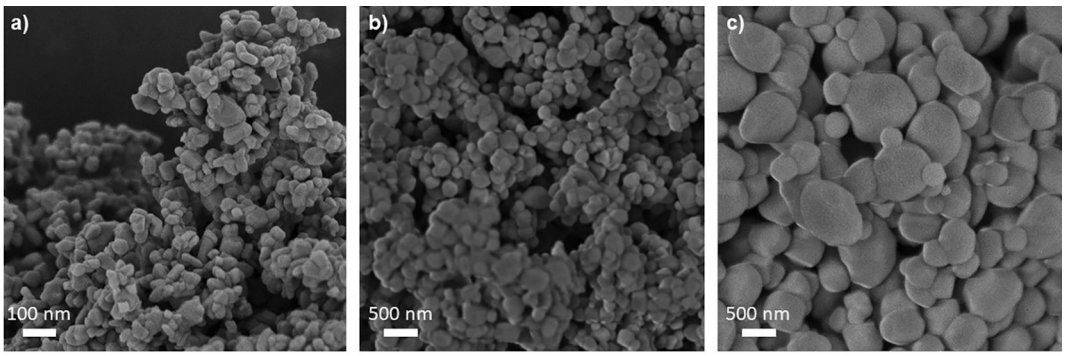

Fig. 2. SEM images of a) NA, b) SMA and c) MA TiO_2.

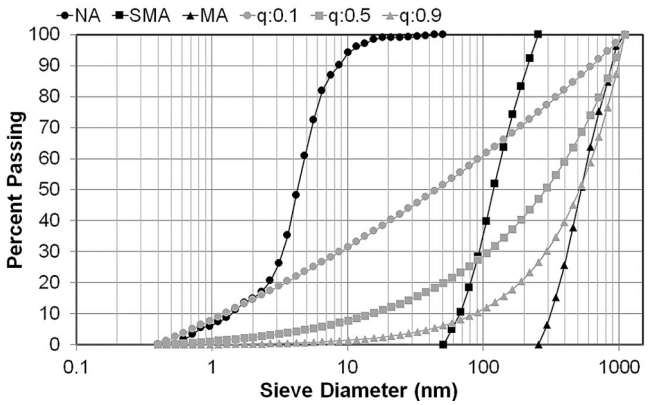

Fig. 3. PSD curves of NA, SMA, MA TiO_2 powders and TiO_2 powders with varying PSD moduli.

2.3. Mixing Process, specimen preparation and testing

All mixing was conducted with an Vibra-Cell ultrasonic mixer with a 25 mm diameter (Fig. 4.a) and a planetary-type laboratory mixer with a 4-liter capacity (Fig. 4.b). To investigate the effects of PSD accurately by providing more homogenous dispersion of TiO_2 in system, the mixing procedure developed/determined in the study of [51] has been followed in this study. The overall mixing process included the following steps: (i) To uniformly disperse powder materials throughout the matrix, surfactant materials (PCE, PAA), TiO_2 powders and water were initially mixed with an ultrasonic mixer for 10 min at a working amplitude of 80% and an energy input of 1900 Joules; (ii) The suspension obtained after ultrasonic mixing was slowly added to a simultaneously operating planetary-type laboratory mixer containing WPC at 100 rpm over 30 s; (iii) Mixing speed was increased to 300 rpm and all ingredients (WPC, TiO_2, water, PCE and PAA) were mixed for another 10 min at 300 rpm.

Mixture performance was evaluated by measuring compressive strength, photocatalytic degradation capability (NO reduction in percentage), hydration kinetics, pore size distribution, and microstructural characterization. For the compressive strength and photocatalytic degradation tests, mixtures were poured into pre-oiled molds and compacted using a vibration table. All specimens were then demolded after curing for 24 h in the laboratory environment and moisture cured in plastic bags at 95 ± 5% RH, 23 °C until testing age. The compressive strength of all mixtures was evaluated according to the ASTM C109 standard. 50 mm cubic specimens were prepared to determine uniaxial compressive strength. Tests were conducted using a loading rate of 0.9 kN/s and the average compressive strength value of three cubic specimens was reported for each curing age of 2, 7, and 28 days.

The dynamic test method was used as in study of [51] to obtain the NO degradation capability of the specimens. In this method, gas passes continuously throughout a test unit at a constant flow rate by interacting with the surface of the specimen and the difference in gas concentration between the system inlet and outlet, which is directly related to photocatalytic efficiency, is monitored by measuring simultaneously in real time. Details of the equipment used to measure NO reduction capability can be found in Fig. 5. To determine photocatalytic efficiency of the mixtures, 50 × 100 × 100 mm prismatic specimens were prepared separately for each curing age of 7, 28 and 90 days. A flow of 1000 ± 50 ppb of NO gas was introduced at a rate of 3.0 l/min, from a 5 mm spacing between the 50 ± 1 cm^2 specimen surface and UV permeable quartz glass positioned above a closed reaction cabinet. UV light with an intensity of 10 W/m^2 was dropped on the specimen surface with two 18 W UV-A blue lamps and one 36 W (UVA-1) white lamp. NO gas entering the system was moistened with a humidifying bottle to reach 50–60% humidity level. In addition, NO gas flowing through the system was diluted

Fig. 4. a) Ultrasonic mixer and b) planetary-type laboratory mixer.

Table 3
Mixture Proportions (values are in g).

Mixture #	ID	PSD Modulus (q)	WPC	TiO_2 MA	SMA	NA	Water	PAA	PCE
1	M0	–	2000	–	–	–	700	10	10
2	MNA	–	1900	–	–	100	700	10	10
3	MSMA	–	1900	–	100	–	700	10	10
4	MMA	–	1900	100	–	–	700	10	10
5	MQ0.1	0.1	1900	25.0	23.5	51.5	700	10	10
6	MQ0.5	0.5	1900	53.1	27.1	19.8	700	10	10
7	MQ0.9	0.9	1900	73.5	20.4	6.1	700	10	10

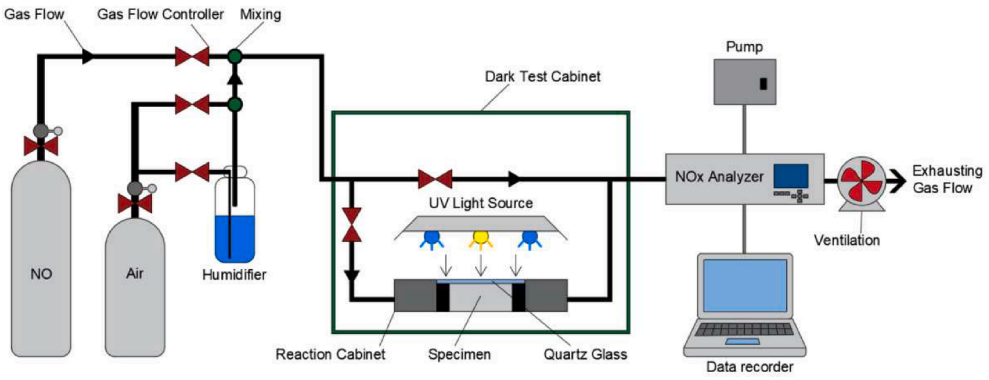

Fig. 5. Schematic view of the photocatalytic testing system.

from 100 ppm to 1 ppm using dry air to ensure proper flow rate. Thermo Scientific Model 42i NO analyzer was used continuously to measure change in NO concentration. To ensure reliable testing under consistent conditions and to prevent the manipulative effects of humidity on photocatalytic efficiency reported by Cassar et al. [52], Dylla et al. [53], and Seo and Yun [16], all specimens were dried in an oven at 45 °C for 48 h before testing. The testing surface of the specimen was then sanded and cleaned, and the specimen was placed in the reaction cabinet, where its upper surface could be illuminated with UV light. To adapt the specimen to the test environment, it was kept under active UV-light sources for four hours without any gas flow through the system. After this process, UV light sources were switched off and pre-adjusted gas flow was introduced to the system. The UV light sources were turned on at least 10 min after the gas concentration remained constant. Under the influence of UV irradiation, photocatalytic specimens started to reduce the NO concentration of flow. The test was performed until the lowest point at which NO concentration remained constant as a result of photocatalytic degradation reactions on the specimen. After that point, UV lights were turned off and gas flow was continued until NO concentration reached its initial level again. At the end of the tests, in order to determine the photocatalytic performance of the cementitious systems, the NO_x and NO reduction, and NO_2 formation (%) values, which were calculated according to Equations (2), (3), and (4), respectively, were obtained. Furthermore, for the purpose of determining the photocatalytic efficiency of the system, selectivity that expresses the ratio of degraded NO that ends up as innocuous nitrate rather than toxic nitrogen dioxide is used and is derived according to Equation (5) [54–55].

$$NO_{xred}(\%) = \frac{NO_{xi} - NO_{xf}}{NO_{xi}} \times 100, \quad (2)$$

$$NO_{red}(\%) = \frac{NO_i - NO_f}{NO_i} \times 100, \quad (3)$$

$$NO_{2for}(\%) = \frac{NO_{2f} - NO_{2i}}{NO_i} \times 100, \quad (4)$$

$$S(\%) = \frac{NO_{xred(\%)}}{NO_{red(\%)}} \times 100, \quad (5)$$

where NO_{xred} (%), NO_{red} (%), and NO_{2for} (%) are NO_x reduction, NO reduction and NO_2 formation, respectively; NO_{xi}, NO_i, and NO_{2i} are of the initial concentrations in order of NO_x, NO, and NO_2; and NO_f, NO_f, and NO_{2f} are the final concentrations of the NO, NO, and NO_2, respectively; finally, S (%) is the system selectivity.

Hydration kinetics of cementitious mixtures were examined using a TAM Air Microcalorimeter in isothermal conditions at 25 °C, in accordance with the practice of ASTM C 1679–17. The fresh pastes were immediately placed in plastic with closed lids and the ampoules were transferred into the calorimeter. Ampoules were placed into the calorimeter within 2 min of the end of mixing. Thermal power (as mW/g of total powder present in the cement paste) was recorded for 72 h to measure rate of hydration (rate of heat evolution). Cumulative heat of hydration curves of the cementitious pastes were also obtained as area under rate of hydration vs. time curves.

The mercury intrusion porosimetry (MIP) technique was used to characterize porosity and pore size distribution of TiO_2-based cementitious systems. First, 28-day-old prismatic specimens used for photocatalytic degradation tests were broken into small pieces, with sizes between 7 and 10 mm. The specimens were then dried in an oven at 50 °C for 1 day and the MIP test was conducted on the dry specimens. The instrument used for MIP testing (Quantachrome Corporation, Poremaster 60) had a pressure capacity of 380 MPa (55000 psia) with a contact angle of 140°.

Microstructural characterization of TiO_2-based cementitious systems were investigated with scanning electron microscopy observations coupled with energy-dispersive X-ray spectroscopy (SEM/EDX) (Tescan-GAIA3 + Oxford XMax 150 EDS) to clarify their morphologies and elemental compositions. For this purpose, specimens were obtained from 28-day-old prismatic specimens used for photocatalytic degradation tests. To do that, tested surface of the photocatalytic specimen was firstly sanded and cleaned. After that, the specimen was broken into small pieces and samples were randomly selected from among the broken pieces. SEM/EDX analyses were conducted on these specimens after being oven-dried overnight. SEM micrographs were captured, and the elemental compositions of the sections viewed were analyzed by SEM-EDX mapping.

3. Experimental results

3.1. Hydration kinetics

Isothermal calorimetry was used to examine the hydration of cementitious pastes, using 0.35 water-to-powder ratio at 25 °C to observe the influence of the PSD of anatase-phase TiO_2 on hydration kinetics. Hydration rate and cumulative heat of hydration of cementitious pastes are presented in Fig. 6. As seen from Fig. 6-a, although M0 (reference specimen non-containing TiO_2) was not the specimen which reached rate of hydration peak earliest, the highest rate of hydration peak value was obtained from this specimen. This result can be attributable to the relatively higher cement content of the reference specimen compared to those of TiO_2-substituted specimens, which will be detailed in compressive strength results section (Section 3.2).

Among the non-optimized specimens (MNA, MSMA, MMA), NA addition resulted in an earlier and higher rate of hydration peak than SMA and MA, probably due to a more effective nucleation effect provided by significantly smaller particles of NA (Table 2). Incorporating nano materials with extremely small particle size has a hydration agitation and acceleration effect [56–59]. This caused higher heat of hydration for the cementitious system containing NA than for the pastes

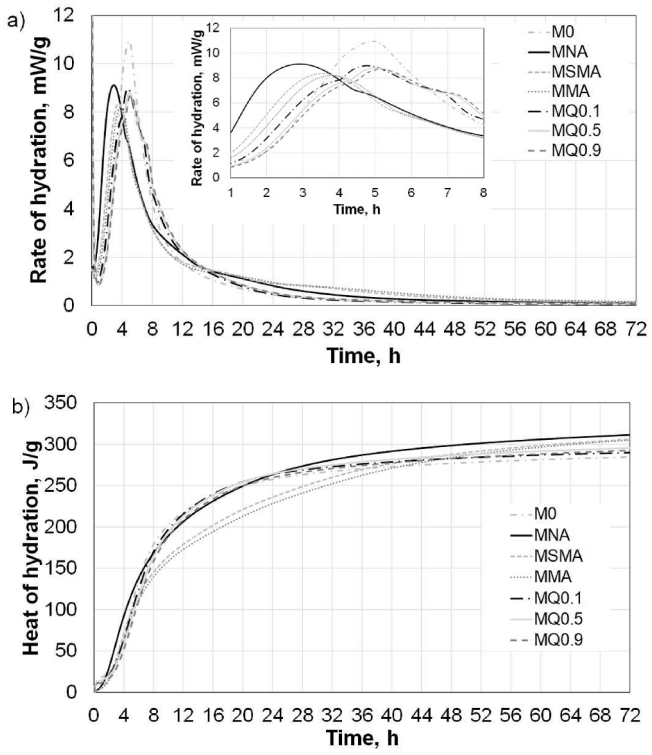

Fig. 6. a) Rate of hydration and b) heat of hydration of cementitious systems with variable PSD of anatase TiO_2.

with SMA and MA, especially between 8 and 48 h of hydration (Fig. 6-b). However, the NA, SMA and MA heat of hydration values were similar at the end of 72 h of hydration. On the other hand, cementitious systems containing a combination of NA, SMA, and MA TiO_2 particles with varying PSD moduli exhibited a maximum rate of hydration comparable to that of the paste with only NA indicating similar seeding/nucleation effects. However, the apparent initial retardation effect—where a longer induction period is observed but without a reduction rate of peak heights for the MQ0.1, MQ0.5 and MQ0.9 may be attributed to retardation of cement grains dissolution because of residual inorganic substances. Knowing that some inorganic (SO_4^{2-}, CO_3^{2-}, PO_4^{3-}, and F^-) materials have an adverse effect on early dissolution rate [60]. In this regard, sulfate ions, coming from extracting and purifying process, on TiO_2's surface may be dissolved into C_3S particles, causing dissolution to be delayed [61–62]. The reason why shifted peak observed by MQ0.1, MQ0.5 and MQ0.9 were related with retardation effects of residual inorganic materials. However, these retardations were not effective on non-optimized TiO_2 used paste mixtures. This could be attributed to effects of PSD which lead more densify structure and covering more cement grain in fresh stages, hence results more retardation effects and less dissolution of particles in initial duration.

When comparing the influence of PSD modulus on the rate and heat of hydration, increasing PSD modulus of TiO_2 particles from 0.1 to 0.9 made no considerable difference. Besides, TiO_2 addition with varying PSD moduli resulted in a higher heat of hydration than SMA and MA TiO_2 for hydration time of up to 48 h. However, the reverse was true thereafter. This finding indicates that using nano-, submicron- and micron-size particles, mixed to provide varying PSD moduli, is highly effective on the rate and total heat of hydration at early periods before 48 h. Furthermore, anatase-TiO_2 with varying PSD moduli caused a small shoulder formation in the rate of hydration curves at around 8 h. This kind of shoulder formation in the deceleration stage of the main hydration peak is generally associated with the conversion of AFt to AFm [63]. Earlier conversion of AFt to AFm, in the case of anatase-TiO_2 with varying PSD moduli, could be attributed to the specific influence of PSD on the hydration of calcium aluminates, which cause earlier conversion of AFt to AFm.

3.2. Compressive strength

Fig. 7 illustrates the compressive strength test results of each mixture for different curing ages. MNA, MSMA, MMA were designed to reveal the effect of the particle size of TiO_2 powders on the performance of cementitious systems. In addition, MQ0.1, MQ0.5, MQ0.9 were designed to better understand the effects of PSD optimization on TiO_2 particles. Due to ongoing hydration reactions, the extended aging/curing resulted in continuous increments in the compressive strength results, irrespective of mixture parameters. MSMA showed the highest strength increase at 33.7%, from 2-day to 7-day curing age. Between 7-day and 28-day curing ages, strength increases slowed for all mixtures. The highest compressive strength test results were recorded from M0 specimen (reference specimen non-containing TiO_2) for each curing age with the values reaching 59.32 MPa for 2-day-old specimens, 71.33 MPa for 7-day-old specimens and 85.30 MPa for 28-day-old specimen. In the available literature, it was reported that the mechanical performance of cementitious systems can be improved with the incorporation of different nano materials up to a certain nano-material utilization rate beyond which decrements or negligible increments can be noted [64–65]. In the study of Jimenez-Relinque et al. [66], incorporation of 2% TiO_2 (by mass of cement) reduced the compressive strength of the cementitious systems. In this regard, considering relatively higher incorporation rate of TiO_2 powder in this study (5% of total weight of powder material), the relatively lower compressive strength results of the TiO_2-incorporated systems (especially of MNA) compared to that of reference specimen (M0) can be attributed to the dilution effect (diminution of cement). The addition of inert TiO_2 powders resulted a less amount of presence of reactive cement (in percentage) in the mixtures decreasing the rate/amount of hydration products manufactured and causing lower compressive strength [65–67].

Among the non-optimized specimens (MNA, MSMA, MMA), it was evident that those containing nano-sized TiO_2 (MNA) showed the highest compressive strength results for each curing age. The compressive strength values of MNA for 2-day, 7-day and 28-day curing ages were 55.40, 66.00 and 77.63 MPa, respectively. The probable reason for this behavior is that nano-sized powders create higher density due to the filler effect arising from comparatively smaller particle size [68]. This behavior can also be attributed to the seeding effect, which is the

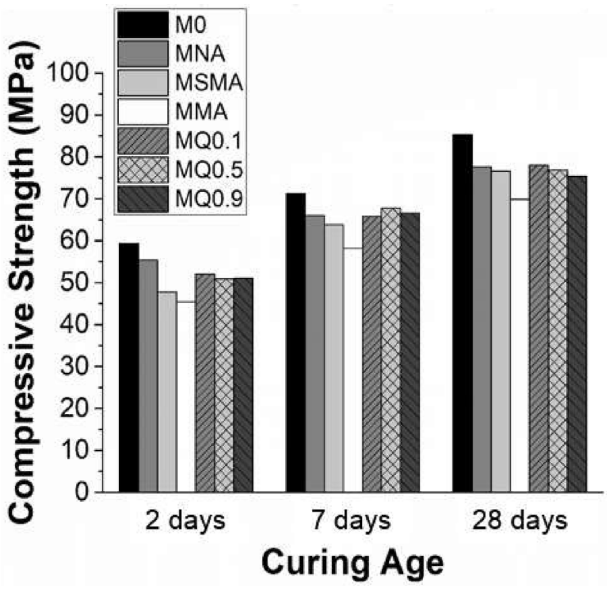

Fig. 7. Compressive strength test results.

formation of additional area (nucleation sites) due to the extremely fine particle size of nano materials (and thereby their high surface area) that can pull unhydrated cement particles towards themselves, resulting in more suitable places for the precipitation of hydration product [69–70].

MMA showed the lowest compressive strength performance among all tested mixtures for each curing age, most probably because of the lower capability of the micron-sized TiO_2 particles in terms of refinement of pore size structure in the paste due to their coarser structure and thereby lower surface areas. In the PSD-optimized specimens (MQ0.1, MQ0.5, MQ0.9), although there was no significant difference in their compressive strength values, MQ0.1 had the highest compressive strength values at approximately 52.10 (2-day), 65.82 (7-day) and 78.01 MPa (28-day), for almost all curing ages except for 7 days. The lowest compressive strength obtained after 28 days of curing among PSD-optimized specimens was 75.37 MPa for MQ0.9. When all results (obtained from TiO_2-incorporated mixtures) are evaluated together and MMA results are excluded, the differences in compressive strength results of mixtures at 28 days was not significantly evident, and compressive strength test results were 76–79 MPa for tests carried out on all TiO_2-incorporated mixtures after 28 days.

3.3. Photocatalytic performance

The photocatalytic activity of 5% anatase-phase TiO_2-substituted cementitious systems was tested to assess the effects of single or combined utilization of three different size ranges of TiO_2 particles on the photocatalytic degradation capability of cementitious systems. Fig. 8 shows NO_x, NO, and NO_2 concentration profiles obtained during the NO degradation tests under illumination. In addition, NO_x and NO degradation and NO_2 formation rates (in percentage) of the developed systems together with the system selectivity values are summarized in Fig. 9 for easy comparison of photocatalytic performances of the specimens. When the degradation rates of 7-day, 28-day and 90-day-old specimens are evaluated, it can be clearly seen that the NO_x degradation rates of MNA were the highest for each curing age. Although using nano-sized materials in the cementitious systems triggers agglomeration problems caused by the high surface interactions due to the particles' high surface area and energy [71], specimens containing nano-sized TiO_2 powder had comparatively high photocatalytic degradation capability. This can be attributed to the easy current transfer capability of the nano-sized TiO_2 from its surface, especially when uniform distribution was guaranteed [9,12,72].

Due to the fact that photocatalytic reactions occur at the surface of the photocatalyst and photons are captured from the surface of materials [73], it is also possible to state that the photocatalytic activity directly depends on the total surface area of the photocatalyst where UV irradiation is reached and on the grain size of the photocatalyst affecting this area, and therefore nano particles can provide maximal photocatalytic surface area accessible to polluting substances. However, the microstructure of cementitious systems incorporating TiO_2 particles is significantly influential on the dispersion of TiO_2 particles throughout the surface where the photocatalytic reactions occur and thereby on the performance of these systems. On the other hand, MSMA and MMA showed considerably lower photocatalytic degradation performance than MNA, with the differences in degradation results becoming significantly more pronounced with longer curing periods. Among the PSD-optimized specimens, photocatalytic degradation rates of MQ0.9 were the highest for all curing ages and after that, in decreasing order, those of MQ0.5 and MQ0.1. Photocatalytic degradation rates of all specimens exhibited a decremental trend starting from 7 to 90 days. This time-dependent trend may have come from the ongoing hydration reaction, leading to the coating of TiO_2 particles with further hydration product and thereby reducing the presence of TiO_2 materials on specimen surfaces reached by UV irradiation. A more likely reason is that carbonation products, produced by binding carbon dioxide (CO_2) into solid carbonates on the specimen surface or another possible process, cause the specimen surface to be coated [17,33,74]. The rate of decrement in photocatalytic degradation results of non-optimized specimens from 7 to 28 days was more evident than in PSD-optimized specimens. With further aging of specimens beyond 28 days, the rate of decrement in photocatalytic degradation results of MSMA and MMA was significantly higher than in other specimens.

As followed from Fig. 9, different NO_2 formation levels were obtained from the specimens at the end of the photocatalytic reactions. The formation of NO_2 in photocatalytic reactions can be related to the HNO_3 and NO_3^- accumulation on the TiO_2 surface over time, reacting with NO, beyond a threshold value, to form NO_2 [75–76]. Besides, the reactions between NO and O_2 and/or HNO_2 and *OH could be another possible reason of the formation of NO_2 [75–77]. Considering the fact that the toxicity of NO_2 is significantly higher than the primary pollutant NO [78], it was critical to monitor the change of NO_2 levels throughout the photocatalytic reactions, and the system selectivity. When evaluating the system selectivity of the cementitious systems, it was clearly observed that the system selectivity of all specimens exhibited an incremental trend starting from 7 to 90 days. In terms of NO_x and NO reduction, although the MNA specimen containing nano-sized TiO_2 was exhibited better performances, the higher selectivity values were obtained from the PSD-optimized specimens. Therefore, it is possible to state that PSD optimization significantly contributed to enhancement in the photocatalytic efficiency of the cementitious systems by increasing the system selectivity. In the PSD-optimized specimens (MQ0.1, MQ0.5, MQ0.9), although there was no significant difference in their system selectivity values, MQ0.9 had the highest one (%91.1) at the end of the 90-day curing age.

3.4. Pore size distribution

MIP was used to test the pore size distributions of 5% TiO_2-substituted cementitious systems containing NA, SMA, MA TiO_2 particles individually or in combination and with varying PSD moduli, at the age of 28 days. MIP was also performed on reference specimen (M0) for comparison. The current pore size classification proposed by the International Union of Pure and Applied Chemistry (IUPAC) was used to describe the pore structure of the cementitious system [79]. This proposed classification classifies the pores into three groups according to their sizes, including macropores, over 50 nm; mesopores, from 50 to 2 nm; and micropores, under 2 nm. According to studies available in the literature, voids larger than 50 nm are, more influential on impermeability and strength characteristics of cement-based systems, whereas voids smaller than 50 nm are more influential on drying shrinkage and creep [80–82]. Therefore, in addition to the IUPAC classification, in this paper, pores were divided into two categories: pores larger than 50 nm termed as pores above 50 nm and pores smaller than 50 nm termed as pores below 50 nm. Total porosity (% of volume) of specimens is presented in Fig. 10. Pore size distribution percentages and curves of all specimens are illustrated in Fig. 11-a and 11-b, respectively. As indicated in Fig. 10 and Fig. 11, reference specimen (M0) had the lowest total porosity value (3.9%) and all pores available in this specimen were smaller than 50 nm, evidencing the highest compressive strength results of the M0 specimen. The figures also show that almost all pores dispersed throughout MNA were smaller than 50 nm. Furthermore, a total porosity value of 4.0% for MNA (Fig. 10) reveals that MNA has a relatively low pore volume compared to the other single-size TiO_2-substituted specimens (MSMA and MMA). As the size of TiO_2 incorporated to the matrix got coarser, the volume of pores smaller than 50 nm formed in the matrix decreased. The rate of pores, ranged between 0 and 50 nm, dispersed throughout MSMA and MMA was at 87.5% and 47.4% of the total amount of pores, respectively. Moreover, the total porosity values of these mixtures were 8.6% for MSMA and 10.4% for MMA: higher than that of MNA, as previously mentioned. It is therefore reasonable to state that using NA TiO_2, (the much finer fraction of the TiO_2) leads to better packaging of the grains, as expected and

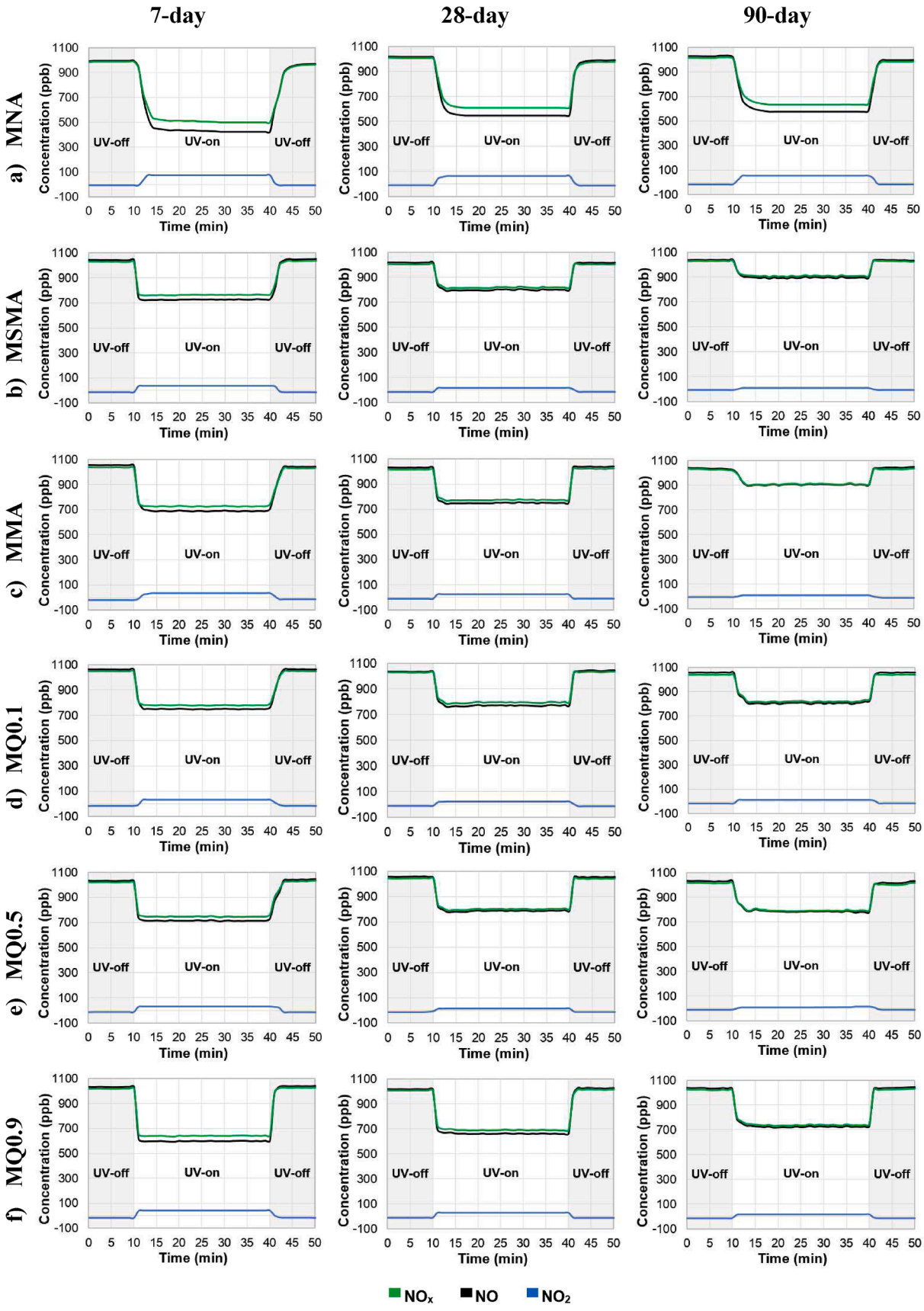

Fig. 8. Variation of NO_x, NO, and NO_2 concentration during each test for 7, 28, and 90 days old specimens.

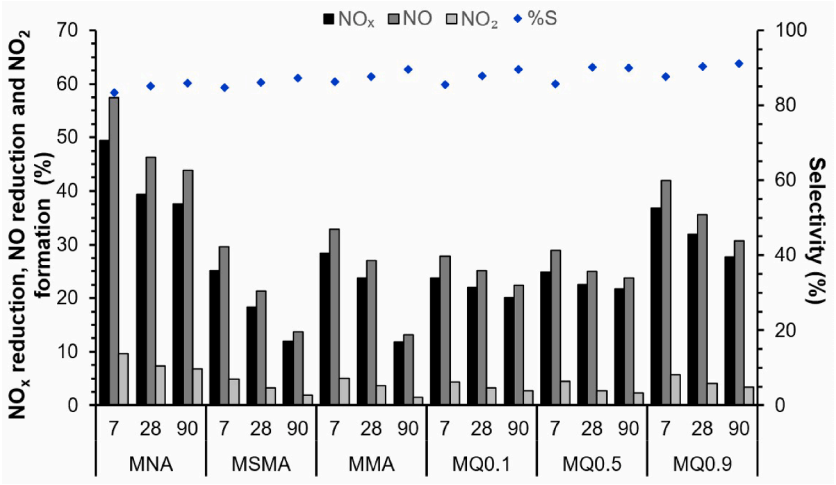

Fig. 9. Variation of NO_x reduction, NO reduction, and NO_2 formation (%) each test for 7-, 28-, and 90-days old specimens and the system selectivity (%).

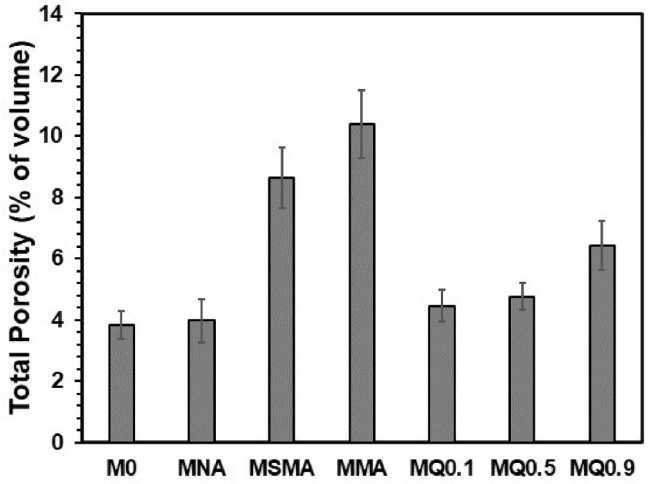

Fig. 10. Total porosity (% of volume) of the specimens.

consequently improves the compactness of the microstructure of specimens because of its filler effect.

The MIP test results of PSD-optimized specimens show that the number of pores below 50 nm in MQ0.1 and MQ0.5 were 100% and the specimen incorporated with TiO_2 using a PSD modulus of 0.9 (MQ0.9) resulted in a lower rate of pores below 50 nm (64.8%) compared to other PSD-optimized mixtures (Fig. 11a). Total porosity values were 4.5%, 4.8% and 6.4% for MQ0.1, MQ0.5 and MQ0.9, respectively; the increase in PSD modulus resulted in an increase in total porosity and proportion of pores above 50 nm. The probable reason for this is that the TiO_2 with the lower PSD modulus ($q = 0.1$) contained a higher proportion of small particles, which can provide more closable smaller interparticle spacing, better fill the voids between larger particles, and improve the packing density of the powder materials (TiO_2 and cement). On the other hand, for MQ0.9, which contained the highest proportion of micron-sized TiO_2 particles among the PSD-optimized specimens, the small-sized TiO_2 content was not enough to fill the voids between large particles and thereby prevented significant improvement in packing density of the powder materials compared to other specimens prepared using a smaller PSD modulus. Consequently, these results show that PSD-optimized specimens have a relatively low amount of porosity compared to non-optimized specimens, except MNA and PSD optimization significantly contributes to the pore refinement of mixtures, although the use of nano-sized TiO_2 alone performed slightly better.

3.5. Microstructural characterization

SEM micrographs with EDX analyses, performed to determine the number of Ti elements dispersed throughout a specific section, were obtained for microstructural characterization studies of TiO_2-based cementitious systems. Analyses of non-optimized and PSD-optimized specimens are shown in Fig. 12 and Fig. 13, respectively. It can be clearly seen from these figures that carbon (C), oxygen (O), calcium (Ca) and silicon (Si) were the primary elements of all specimens, and substantial part of the chemical content of all specimens was composed of Ca and O. The C contents by weight of all specimens were lower than 9%. The Ti contents (by weight %) of MNA, MSMA and MMA were 2.4, 1.7 and 4.9, respectively. For the PSD-optimized specimens, Ti contents (by weight, %) of MQ0.1, MQ0.5 and MQ0.9 were 1.9, 2.2, and 4.9, respectively. Although the amount of photocatalyst located across the surface reachable by UV-radiation has an undeniable influence on photocatalytic performance of cementitious systems, there was no obvious correlation between the amount of photocatalyst and the photocatalytic degradation rate of specimens. Considering that photocatalytic efficiency of TiO_2 particles can be affected by their crystal structure, surface area and particle size [83], the NO degradation results should be associated with the higher presence of small-sized TiO_2 on the UV-reached surface, which resulted in increments in the number of active surface sites and thereby high separation and transfer efficiency of surface charge carriers.

EDX elemental mapping images of relevant specimens are also illustrated in Figs. 12-13: red corresponds to Ti atoms and green to Ca atoms. One of the main elements (Ca) was detected in all regions of the specimens. Based on the evidence in these images, Ti elements have more uniformly dispersed throughout the PSD-optimized specimens. For the non-optimized specimens, the distribution of the Ti atoms on the surface of MNA and MMA was also generally homogeneous, although some irregularities in the dispersion of the TiO_2 particles were seen in the microstructure of MSMA specimens.

4. Discussions

In term of mechanical properties, in the non-optimized specimens, the compressive strength of the MNA surpassed all other mixtures for all curing ages. This finding has been reported by several other researchers in the literature. They attributed it to various enhancement influences of nano-scale materials on microstructural and mechanical properties in favor of obtaining a denser matrix. Well-graded ingredients stimulate the hydration process due to their high surface area, resulting in nucleation sites bonding with cement hydrates [58,84], hydration

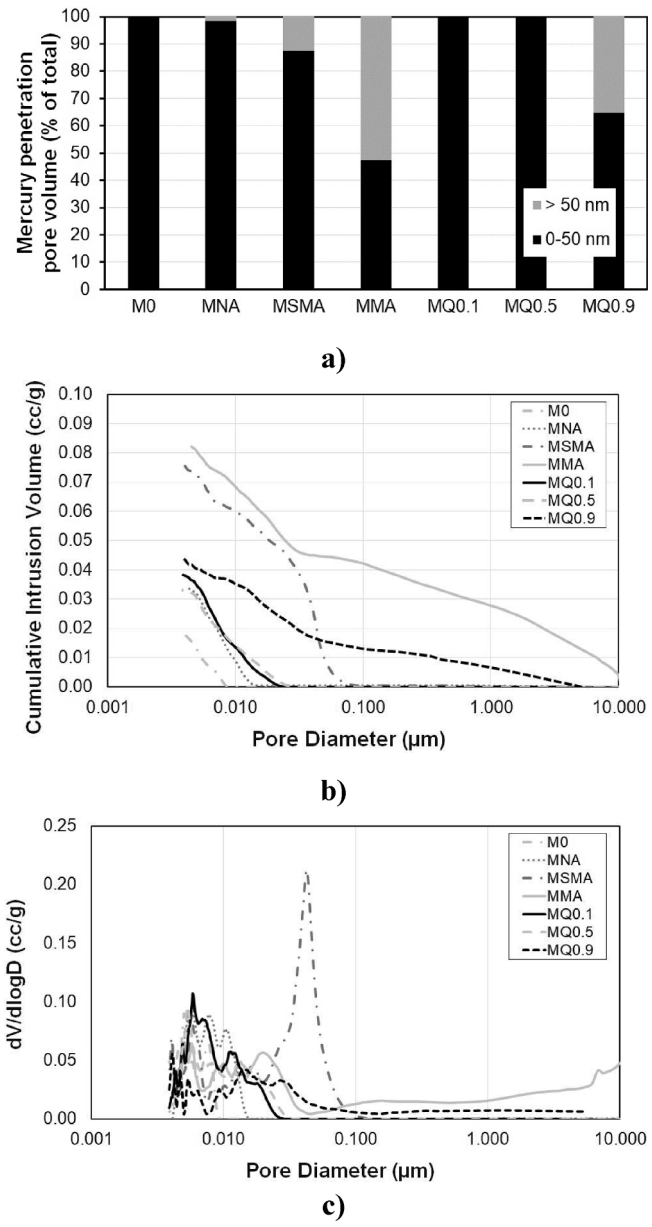

Fig. 11. a) Mercury penetration pore volume (% of total), b) Pore size distribution curves of specimens, c) dV/dlogD (cc/g).

agitation, acceleration effect [56–59] and filler effect, resulting in relatively better particle packing of constituents [56–57]. The hydration kinetics results of cementitious pastes shown in Fig. 6 show that using nano-sized TiO_2 (NA) caused an enhanced/accelerated degree of hydration reaction (kinetics) of the cementitious paste (larger peak magnitude and earlier time of peak occurrence) owing to its considerably fine structure providing significant surface energy. This acceleration confirms that using nanoparticles (NA) provides higher early-age strength. As the particle size of the TiO_2 in cementitious systems increased (among specimens characterized by single use of TiO_2 particles), the peak occurrence time increased and the peak magnitude decreased. This situation is in accordance with the results of compressive strength, which determined that increasing particle size decreases strength. Although the MNA showed highest compressive strength performances among non-optimized specimens for each curing age, the incorporation of nano-sized TiO_2 reduced the compressive strength results of the cementitious system considering relatively higher compressive strength performance of the TiO_2 non-containing specimen (M0). In this regard, it is possible to state that the decremental effect of the decrease in the reactive cement content of MNA, because of replacement of cement with inert TiO_2, on mechanical performance was more dominant than the enhancing effects of the nano materials (detailed above) incorporation into cementitious systems. It should be also stated that although, at the end of the 48 h, heat of hydration released from MNA was higher than the reference mixture, the compressive strength results were inconsistent with this case. The possible reason of this situation can be related with (i) differences in the consistency of the mixtures due to the different sized TiO_2 content, (ii) formation of heterogenous reaction product for faster hydration at the early age and (iii) differences in the hydration products because the possible effects of TiO_2 existence.

Of the PSD-optimized specimens, MQ0.1 showed better compressive strength results than the other mixtures at the end of 28 days. It is especially noteworthy that the compressive strength of MQ0.1 is higher than that of MNA, which can be attributed to its well-graded PSD achieving high particle packing density. When the hydration kinetics results shown in Fig. 6 are evaluated, it can be clearly seen that using TiO_2 with varying PSD moduli resulted in a retardation of peak occurrence compared to the single-sized TiO_2 (longer time of peak occurrence) due to retardation of early dissolution as a result of residual inorganic chemicals [62] and better covering capability of PSD-optimized TiO_2 particles. As the PSD modulus increased, the peak occurrence time increased and also its magnitude decreased due to decrement in seeding and nucleation capability with increased coarser TiO_2 particles. The 28-day compressive strength results of optimized specimens were consistent with these results. Peak magnitude values (maximum rate of hydration) of cementitious systems containing a combination of NA, SMA, and MA TiO_2 particles with varying PSD moduli were higher than those in systems containing SMA or MA TiO_2, and lower than in those containing NA TiO_2. The cumulative heat of hydration values of single-size TiO_2-substituted cementitious systems at the end of 72 h of hydration were higher than those of systems containing a combination of NA, SMA, and MA TiO_2 particles with varying PSD moduli. As a result, considering the higher peak magnitude value, the earlier peak occurrence and the higher cumulative heat of hydration of cementitious system containing NA TiO_2 at the end of 72 h of hydration, it can be clearly stated that MQ0.1′s relatively high compressive strength compared to MNA was geometry-related (physical) rather than chemistry-related (chemical), and PSD optimization with PSD modulus of 0.1 provided the highest particle packing density, as mentioned earlier.

Considering all of these results, it can be clearly stated that although the difference between compressive strength results was not significantly prominent, meaningful differences were noted for 28-day-old specimens. Less pronounced effect of the modification/optimization of the PSD of TiO_2 powders on the compressive strength of specimens containing PSD-optimized powders can be attributed to the relatively wide range of particle sizes of NA and SMA TiO_2 batches, resulting in naturally good particle grading, thereby positively affecting the mechanical properties of specimens. Although it was minimally effective in increasing compressive strength for this study, the advantages of PSD-optimization of TiO_2 powders in tailoring microstructural properties are also likely to improve compressive strength results of mixtures with PSD-optimized powders over those containing TiO_2 powders with a narrower range of particle sizes.

The most important element of this study is the enhancement of the NO_x degradation efficiency of mixtures through optimization of the PSD of TiO_2 powders. As mentioned earlier, the photocatalytic activity of TiO_2 is highly dependent on its size, shape, type, phase and on changes in particle properties [85], and the photocatalytic degradation capability of the nano-sized TiO_2 particles is higher compared to the larger ones [22–27]. It is therefore not surprising that the highest performance in NO_x degradation capability was obtained from MNA for all curing ages. When the EDX analyses of MNA and MMA in Fig. 12(a) and 12(c) are

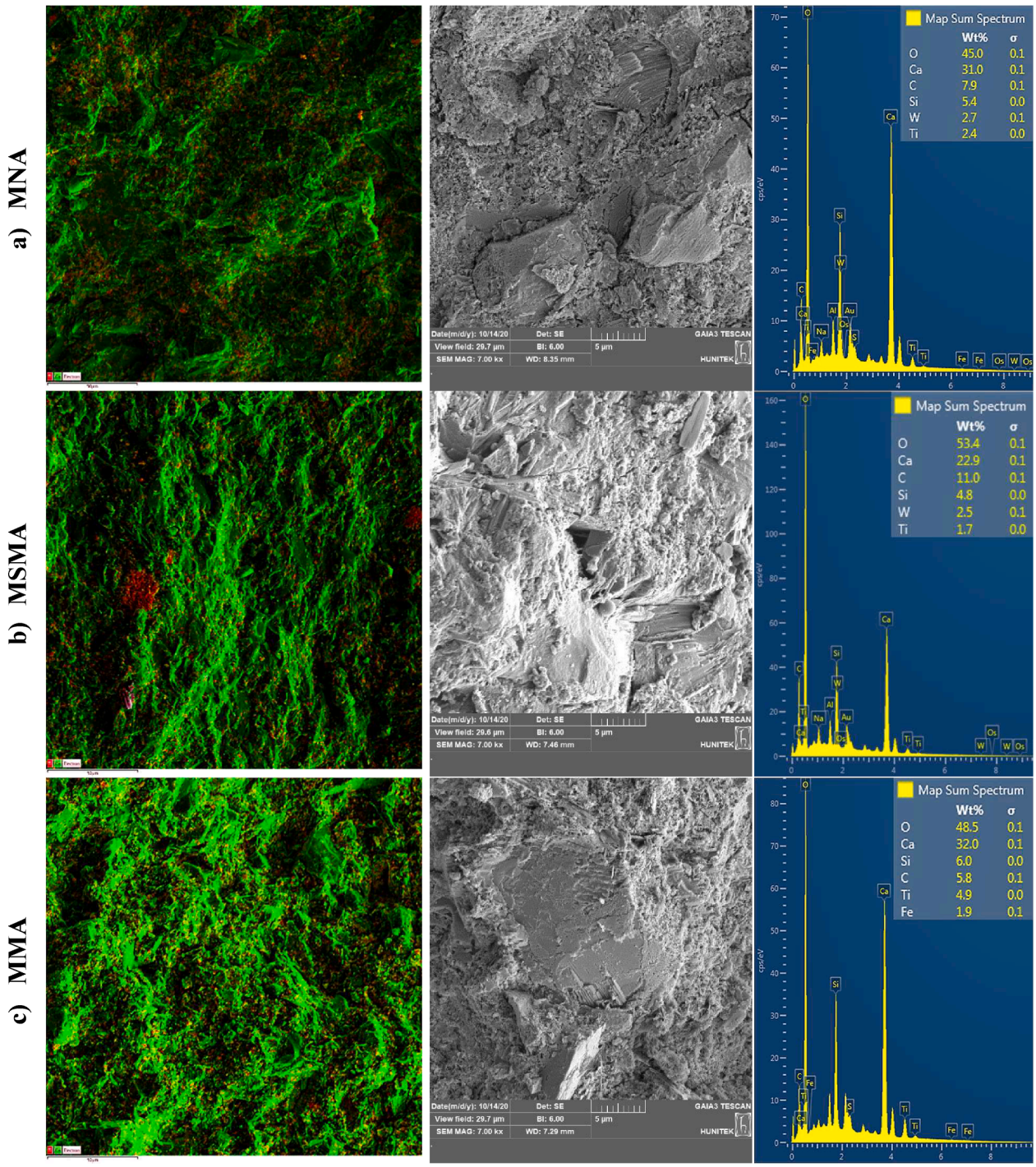

Fig. 12. Representative EDX elemental mapping images and SEM micrographs with EDX spectra of non-optimized specimens.

evaluated, it is evident that the Ti content (by weight %) dispersed throughout the viewed section of MNA (2.4%) was lower than that of MMA (4.9%), possibly due to the denser structure of the MNA. However, higher amounts of the Ti element throughout MMA did not provide higher NO degradation results than in MNA. This result also confirmed that smaller-size photocatalysts provide a more efficient photocatalytic degradation process than larger ones. This was not the case when MSMA and MMA results were compared, which is likely related to the microstructural characteristics of these specimens (explained below). However, it should be kept in mind that EDX results of the equivalent specimens can vary according to the section viewed. On the other hand, for PSD-optimized specimens, MQ0.9 showed better NO_x degradation capability, even though it contained a significantly lower amount of nano-sized TiO_2 than the other PSD-optimized specimens. In addition, whereas the amount of nano-sized TiO_2 in MNA was quite a bit larger than in MQ0.9, a remarkable difference in the nano-sized TiO_2 content was not apparent when comparing NO_x degradation rates of these two specimens. This situation is directly related to specimen microstructure and surface characteristics and may be attributed to the ability of the mixtures, through PSD optimization of TiO_2 particles, to keep distribution and/or the amount of TiO_2 particles optimal throughout the UV-reached surface where photocatalytic reactions occur. Fig. 10 and Fig. 11 show a low amount of total porosity in MNA and more small-size pores compared to the others, both of which indicate good packing

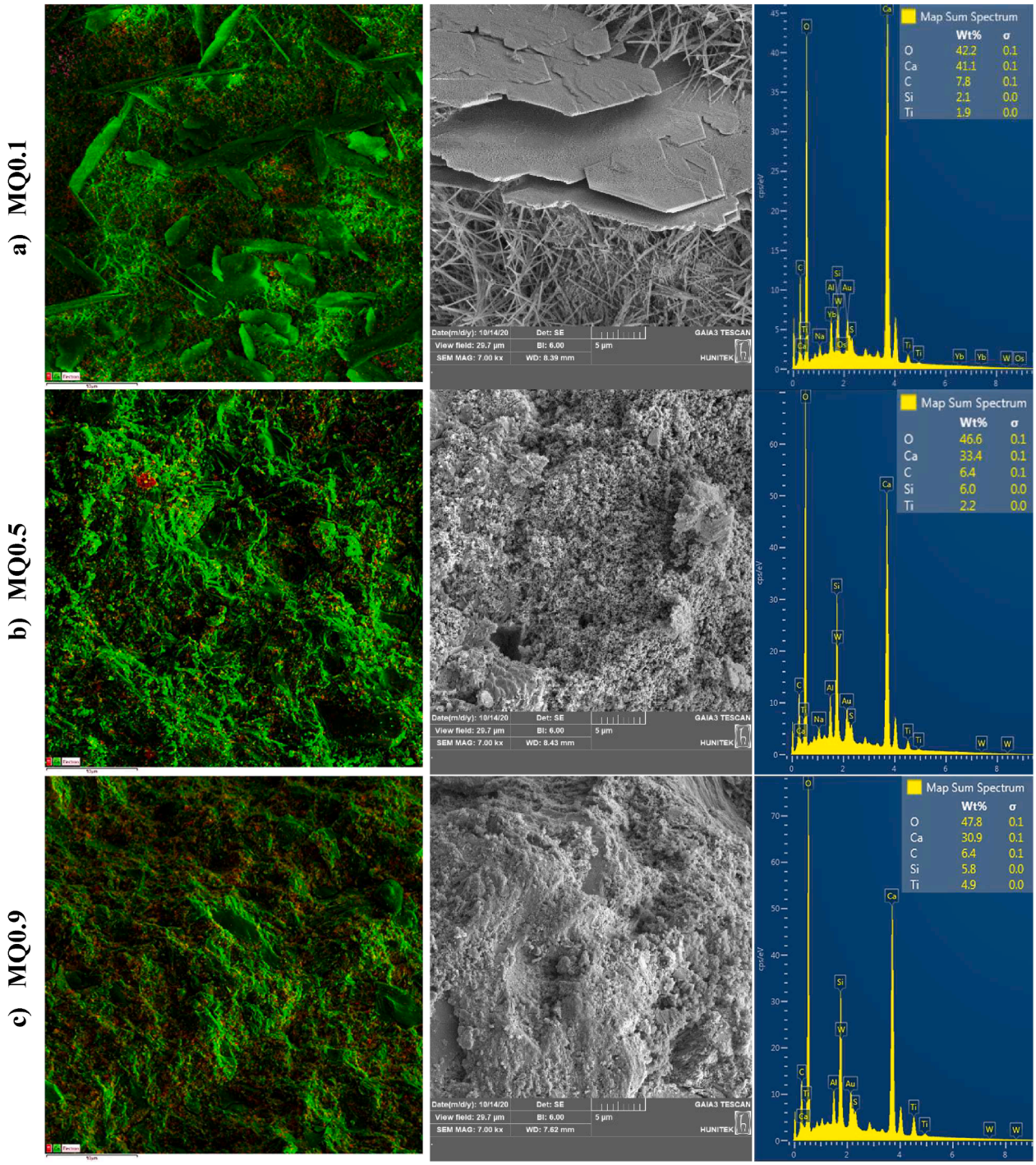

Fig. 13. Representative EDX elemental mapping images and SEM micrographs with EDX spectra of PSD-optimized specimens.

density in favor of particle distribution homogeneity and higher compactness. Therefore, the relatively lower difference between NO_x degradation rates of MNA and MQ0.9 was most probably due to the surface of the nano-TiO_2 particles in MNA being further covered with hydration products. As a result, nano-TiO_2 particles are likely to remain in the dark depths of the denser specimens, resulting in insufficient contact with UV-light and TiO_2 particles and preventing photocatalytic reactions. This situation was also valid for PSD-optimized specimens. Moreover, when evaluating the system selectivity of the cementitious systems, it can be clearly seen that MQ0.9 exhibited relatively higher performance, which means a more efficient NO_x degradation capability.

Although a refined pore structure due to good particle grading caused relatively greater compressive strength, this negatively affected the photocatalytic activity of the mixtures, thereby causing NO_x degradation with low efficiency. Furthermore, the optimal TiO_2 quantities from different-sized TiO_2 batches sufficient for efficient photocatalytic activity were different than those sufficient for mechanical property. In this regard, the most favorable particle packing was provided at a PSD modulus of 0.1 with well-graded TiO_2 particles (MQ0.1), which achieved higher strength results than the other PSD-optimized mixtures, although some natural variations were observed. This can be attributed to the improvement/optimization of the PSD of powder materials in a proper manner, which promoted pore refinement of the microstructure of the cementitious systems, thereby obtaining a relatively denser matrix.

Although MQ0.1 contains higher amounts of more active nano-sized TiO_2, its dense structure resulted in lower photocatalytic efficiency compared to other PSD-optimized specimens. On the other hand, MQ0.9 showed superior photocatalytic efficiency among all PSD-optimized specimens, despite having a small amount of nano-TiO_2. Therefore, it is plausible that the NO_x degradation capability of the mixtures is strongly related to the microstructure characteristics of matrix (as mentioned earlier) although their relationship is quite different than the relationship between microstructure and compressive strength.

MIP test results of MQ0.9 showed 6.4% total porosity and 64.8% pores below 50 nm, the highest total porosity and lowest number of pores below 50 nm among all the PSD-optimized specimens. This means that the PSD modulus of 0.9 provided a considerably higher number of pores above 50 nm, and that the amount/volume of pores dispersed throughout MQ0.9 was relatively higher compared to the other PSD-optimized specimens. Hence higher photocatalytic degradation capability of the MQ0.9 compared to the other PSD-optimized specimens may stem from the larger number of pores limiting coverage of the TiO_2 particles with hydration product. Another possible reason for the better photocatalytic efficiency of MQ0.9 is due to the multiple pore-structure of MQ0.9 homogeneously spread throughout the surface morphology, which causes a large number of TiO_2 particles to be dispersed throughout pore walls for maximum photocatalytic surface area. In addition, larger pores can allow pollutant gas (NO gas) to diffuse into the cementitious matrix more easily, thereby more pollutants participate in the photocatalytic reactions and provide easily reaching of photons to the TiO_2-containing inner parts of the specimens in favor of further contact between the surface of photocatalytic materials and UV irradiation. This situation also evident for MMA and MSMA. Although MSMA contained submicron-sized TiO_2 particles with photocatalytic efficiency that is expected to be higher than in micron-sized TiO_2, the NO degradation capability of MMA at 7 and 28 days was higher than that of MSMA. This can also be attributed to the fact that MMA contained a relatively higher volume of pores, the large majority of which were pores above 50 nm. Fig. 14 shows the relationship between the total porosity (% of volume) and NO degradation rate of specimens. Although MIP tests were carried out on 28-day specimens, total porosity (% of volume) of 28-day old specimens (considering that these reflect the tendency of specimens to form pores), was associated with NO_x degradation results at all ages of relevant specimens.

It can be seen from Fig. 14a and 14b that the general trends of these two graphs are different from each other. According to Fig. 14a (non-optimized specimens), NO_x degradation had an inversely proportional relation to the total porosity of the specimen, whereas the opposite was the case with the PSD-optimized specimens in Fig. 14b. Considering the limitations of using trend lines to show the general trend of specimens, as well as the complexity of this situation due to the presence of many factors affecting the characteristics of the specimens, this requires a deeper, more careful assessment. In this regard, if MNA is excluded, it can be clearly stated that the increased total porosity value contributes positively to photocatalytic degradation capability. MNA not fitting this trend is due to its relatively smaller particle size TiO_2 content, resulting in higher NO_x degradation capability. The photocatalytic efficiency of a cementitious system is significantly related to factors such as physically and chemically effective factors including pore structure and quantity or NO_x degradation capability/efficiency in relation to photocatalyst particle size. When they were more dominant/prominent, the negative effect of comparatively less porosity on photocatalytic efficiency was not dominant enough for MNA to cause lower degradation in the positive effect of finer TiO_2 particle content on photocatalytic efficiency compared to MSMA or MMA. However, this was not the case for PSD-optimized specimens. As mentioned earlier, the relatively higher presence of nano-TiO_2 content could not provide greater NO_x degradation results for PSD-optimized specimens. Increments in total porosity and the presence of pores above 50 nm had a greater effect on NO_x degradation capability of PSD-optimized specimens, indicating that more

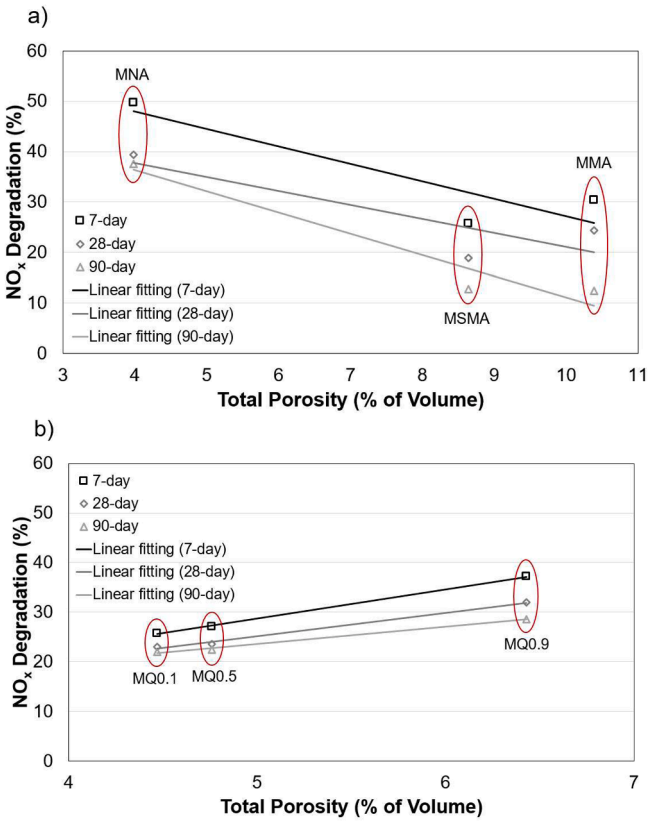

Fig. 14. Relationship between total porosity (% of volume) and NO degradation rate of specimens for (a) PSD non-optimized specimens (b) PSD optimized specimens.

pores could lead to higher photocatalytic efficiency for TiO_2-substituted cementitious systems.

Matrix transformations that also take place on the surface of the cementitious matrix with prolonged age mostly affect the photocatalytic activity of the specimens. The results of PSD-optimized specimens showed that optimizing the PSD of TiO_2 particles can limit the decrease in photocatalytic performance with further aging, such limitation was more pronounced for specimens with denser structure. These results revealed that a TiO_2 batch optimized with the proper PSD modulus could be used as a long-term, stable and efficient photocatalyst for air purification, with optimum performance in practical use.

Of the non-optimized specimens, those with denser structure (MNA) also showed more stable photocatalytic efficiency over time. This could be because the dense structure of the specimens limits further coating of the already coated TiO_2 particles over time with further hydration and leads to less sensitivity to carbonation because their network of interconnected pores is more significantly developed than in mixtures with denser structure. Low efficiency of MSMA and MMA in terms of aged photocatalytic efficiency can be also attributed to their relatively high pore volume content. This situation was also valid for PSD-optimized specimens, even though it was more pronounced for non-optimized specimens. MQ0.9, which has highest pore volume content among the PSD-optimized specimens, also showed more unstable photocatalytic degradation performance over time than denser PSD-optimized specimens.

High porosity allows further penetration of carbonation in deeper layers. By sanding the surface of specimens with lower pore volume, most of the carbonation product can be removed from the UV-reached surface, thereby freeing it of TiO_2 particles. In this way, photocatalytic reactions occurred due to a surface being free from carbonation product, and more stable specimens were obtained depending on time. Further

investigations are necessary to clarify the effect of carbonation on photocatalytic efficiency of cementitious systems by considering its relationship with the pore structure characteristics of these systems.

5. Conclusions

This study investigated the effect of particle size distribution (PSD) and optimization of TiO_2 particles on the mechanical and photocatalytic efficiency of cementitious systems. Specimens were prepared with single-use nano-sized, submicron-sized and micron-sized TiO_2 particles and co-utilizing them with different PSD moduli. This assessed the effects of PSD optimization with different PSD moduli on mechanical and physical properties of mixtures based on compressive strength, porosity and pore size distribution, hydration kinetics and NO_x degradation capability of cementitious systems. The following conclusions are based on the findings of this study:

- The compressive strength of the reference mixture without TiO_2 (M0) was the highest among all mixtures, regardless of the curing ages. Among the TiO_2-incorporated mixtures, modification/optimization of the PSD of TiO_2 powders with a proper PSD modulus provided relatively better mechanical performance by ensuring high compactness. Specimens prepared by using TiO_2 powder optimized with the PSD modulus of 0.1 performed comparatively better under compressive strength test than other non-optimized and PSD-optimized specimens at the end of 28 days.
- Although specimens containing nano-sized TiO_2 particles showed the highest photocatalytic activity, a comparatively high efficiency cementitious system in terms of NO_x degradation capability was obtained with PSD optimization of TiO_2 powders, probably due to the pore structure. High photocatalytic efficiency was obtained by using a considerably smaller number of nano TiO_2 particles, which have higher photocatalytic activity than larger ones. By optimizing the PSD of TiO_2 particles, lower decrements in NO_x degradation of mixtures over curing time were also achieved. Furthermore, PSD optimization increased the system selectivity, which proves that PSD optimization contributes to the enhancement in photocatalytic efficiency of the TiO_2-incorporated cementitious systems.
- When results related to hydration kinetics are evaluated separately for the optimized and non-optimized cementitious systems, the system with higher peak magnitude value, earlier peak occurrence, and higher cumulative heat of hydration (at the end of 72 h of hydration) showed lower total porosity formation (% of volume) and less pores above 50 nm formation. A more pronounced enhanced/accelerated hydration process was obtained by using nano-sized TiO_2 particles, resulting in the decrease of total volume of pores and the formation of pores above 50 nm. When all results are compared, it is clear that although an enhanced/accelerated hydration reaction (kinetics) was not obtained, the formation of a dense structure with proper particle packaging through ideal PSD optimization (for $q = 0.1$) prevented the formation of pores above 50 nm and thereby provided higher compressive strength.
- The pore structure of the TiO_2-substituted cementitious systems is significantly influential on their mechanical and photocatalytic properties. Although higher volume of pores (especially pores above 50 nm) increases the NO_x degradation capability of specimens, it causes higher rate of decrements in photocatalytic degradation capability with increasing curing time. In addition, a higher proportion of pores reduces compressive strength of the cementitious systems. The optimum PSD value may differ depending on the performance expected from the specimens. While the PSD value, which causes an optimum packing density and very dense microstructure, was beneficial in terms of compressive strength, it provided a less effective photocatalytic activity.
- Increasing the number of TiO_2 particles across the surface of specimens that UV rays can reach, is the key parameter in improving the photocatalytic efficiency of cementitious systems, and is significantly related to specimen microstructure. Therefore, the PSD of TiO_2 particles, which is also effective on microstructure, must be considered for the design of photocatalytic cementitious systems.

CRediT authorship contribution statement

Emrah Bahşi: Investigation, Methodology, Writing – original draft. **Oğuzhan Şahin:** Investigation, Methodology, Writing – original draft. **Hüseyin İlcan:** Investigation, Methodology, Writing – original draft. **Burak Uzal:** Funding acquisition, Writing – review & editing. **Muhammed Faruk Günal:** Investigation, Methodology, Writing – original draft. **Gürkan Yıldırım:** Funding acquisition, Data curation, Conceptualization, Writing – review & editing. **Mustafa Şahmaran:** Funding acquisition, Project administration, Supervision, Writing – review & editing.

Declaration of Competing Interest

The authors declare that they have no known competing financial interests or personal relationships that could have appeared to influence the work reported in this paper.

Acknowledgement

The authors gratefully acknowledge the financial assistance of the Scientific and Technical Research Council (TUBITAK) of Turkey provided under projects: 118M197. This publication is a part of doctoral dissertation work by the first author in the Academic Program of Civil Engineering, Institute of Science, Hacettepe University.

References

[1] D. Tristantini, R. Mustikasari, Modification of TiO_2 nanoparticle with PEG and SiO_2 for anti-fogging and self-cleaning application, Int. J. Eng. Technol. 11 (2) (2011) 73–78.
[2] D.M. Chien, N.N. Viet, N.T.K. Van, N.T.P. Phong, Characteristics modification of TiO_2 thin films by doping with silica and alumina for self-cleaning application, J. Exp. Nanosci. 4 (3) (2009) 221–232, https://doi.org/10.1080/17458080902920506.
[3] T.K. Tseng, Y.S. Lin, Y.J. Chen, H. Chu, A review of photocatalysts prepared by sol-gel method for VOCs removal, Int. J. Mol. Sci. 11 (6) (2010) 2336–2361, https://doi.org/10.3390/ijms11062336.
[4] Q. Zhang, J.B. Joo, Z. Lu, M. Dahl, D.Q. Oliveira, M. Ye, Y. Yin, Self-assembly and photocatalysis of mesoporous TiO_2 nanocrystal clusters, Nano Res. 4 (1) (2011) 103–114, https://doi.org/10.1007/s12274-010-0058-9.
[5] S. Anandan, T. Narasinga Rao, M. Sathish, D. Rangappa, I. Honma, M. Miyauchi, Superhydrophilic graphene-loaded TiO_2 thin film for self-cleaning applications, ACS Appl. Mater. Interfaces. 5(1) (2013) 207-212. 10.1021/am302557z.
[6] B.M. Kim, H.M. Yadav, J.S. Kim, Self-cleaning performance of sol–gel-derived TiO_2/SiO_2 double-layer thin films, J. Coat Technol. Res. 13 (5) (2016) 905–910, https://doi.org/10.1007/s11998-016-9804-6.
[7] H.E. Çamurlu, Ö. Kesmez, E. Burunkaya, N. Kiraz, Z. Yeşil, M. Asiltürk, E. Arpaç, Sol-gel thin films with anti-reflective and self-cleaning properties, Chem. Pap. 66 (5) (2012) 461–471, https://doi.org/10.2478/s11696-012-0144-4.
[8] Z. Yuan, B. Li, J. Zhang, C. Xu, J. Ke, Synthesis of TiO_2 thin film by a modified sol-gel method and properties of the prepared films for photocatalyst, J. Sol-gel Sci. Technol. 39 (3) (2006) 249–253, https://doi.org/10.1007/s10971-006-8164-6.
[9] O. Carp, C.L. Huisman, A. Reller, Photoinduced reactivity of titanium dioxide, Prog. in Solid State Chem. 32 (1–2) (2004) 33–177, https://doi.org/10.1016/j.progsolidstchem.2004.08.001.
[10] V. Zivica, A. Bajza, Acidic attack of cement-based materials - a review, Constr. Build. Mater. 15 (8) (2001) 331–340, https://doi.org/10.1016/S0950-0618(01)00012-5.
[11] H. Chen, A. Namdeo, M. Bell, Classification of road traffic and roadside pollution concentrations for assessment of personal exposure, Environ. Model. Softw. 23 (3) (2008) 282–287, https://doi.org/10.1016/j.envsoft.2007.04.006.
[12] J. Zhao, X. Yang, Photocatalytic oxidation for indoor air purification: a literature review, Build. Environ. 38 (5) (2003) 645–654, https://doi.org/10.1016/S0360-1323(02)00212-3.
[13] S. Hager, R. Bauer, G. Kudielka, Photocatalytic oxidation of gaseous chlorinated organics over titanium dioxide, Chemosphere 41 (8) (2000) 1219–1225, https://doi.org/10.1016/S0045-6535(99)00558-5.

[14] G. Hüsken, M. Hunger, H.J.H. Brouwers, Experimental study of photocatalytic concrete products for air purification, Build. Environ. 44 (12) (2009) 2463–2474, https://doi.org/10.1016/j.buildenv.2009.04.010.
[15] S. Wang, H. Ang, O. Tade, Volatile organic compounds in indoor environment and photocatalytic oxidation: State of the art, Environ. Int. 33 (5) (2007) 694–705, https://doi.org/10.1016/j.envint.2007.02.011.
[16] D. Seo, T.S. Yun, NO removal rate of photocatalytic cementitious materials with TiO_2 in wet condition, Build. Environ. 112 (2017) 233–240, https://doi.org/10.1016/j.buildenv.2016.11.037.
[17] J. Chen, C.S. Poon, Photocatalytic cementitious materials: Influence of the microstructure of cement paste on photocatalytic pollution degradation, Environ. Sci. Technol. 43 (23) (2009) 8948–8952, https://doi.org/10.1021/es902359s.
[18] G. Husken, H.J.H. Brouwers, Air purification by cementitious materials: Evaluation of air purifying properties. In International Conference on Construction and Building Technology, Kuala Lumpur, Malaysia, 2008.
[19] M. Hunger, G. Husken, H.J.H. Brouwers, Photocatalysis applied to concrete products-Part 2: Influencing factors and product performance, ZKG international 61 (10) (2008) 76–84.
[20] C. Meng, P. Dong, H. Tian, T. Cheng, J. Li, Y. Liu, X. Yang, M. Xie, X. Chen, X. Xi, Photocatalytic concrete paving block reinforced by TiO2 nanotubes for NO removal, J. Mater. Sci. 55 (29) (2020) 14280–14291, https://doi.org/10.1007/s10853-020-05048-w.
[21] A. Folli, I. Pochard, A. Nonat, U.H. Jakobsen, A.M. Shepherd, D.E. Macphee, Engineering photocatalytic cements: understanding TiO2 surface chemistry to control and modulate photocatalytic performances, J. Am. Ceram. Soc. 93 (10) (2010) 3360–3369, https://doi.org/10.1111/j.1551-2916.2010.03838.x.
[22] M. Anpo, T. Shima, S. Kodama, Y. Kubokawa, Photocatalytic Hydrogenation of CH3CCH with H2O on Small-Particle TiO_2: Size Quantization Effects and Reaction Intermediates, J. of Phys. Chem. 91 (1987) 4305.
[23] L. Cao, A. Huang, F.J. Spiess, S.L. Suib, Gas-phase oxidation of 1-butene using nanoscale TiO_2 photocatalysts, J. Catal. 188 (1) (1999) 48–57, https://doi.org/10.1006/jcat.1999.2596.
[24] L. Cao, Z. Gao, S.L. Suib, T.N. Obee, S.O. Hay, J.D. Freihaut, Photocatalytic oxidation of toluene on nanoscale TiO_2 catalysts: studies of deactivation and regeneration, J. Catal. 196 (2) (2000) 253–261, https://doi.org/10.1006/jcat.2000.3050.
[25] L. Gao, Q. Zhang, Effects of amorphous contents and particle size on the photocatalytic properties of TiO_2 nanoparticles, Scr. Mater. 44 (8–9) (2001) 1195–1198, https://doi.org/10.1016/S1359-6462(01)00681-9.
[26] Y. Ohama, D. Van Gemert, Application of titanium dioxide photocatalysis to construction materials: state-of-the-art report of the RILEM Technical Committee 194-TDP (Eds.), (2011), (Vol. 5), Springer Science and Business Media.
[27] H. He, C. Liu, K.D. Dubois, T. Jin, M.E. Louis, G. Li, Enhanced charge separation in nanostructured TiO_2 materials for photocatalytic and photovoltaic applications, Ind. Eng. Chem. Res. 51 (37) (2012) 11841–11849, https://doi.org/10.1021/ie300510n.
[28] M. Pérez-Nicolás, I. Navarro-Blasco, J.M. Fernández, J.I. Alvarez, Atmospheric NOx removal: Study of cement mortars with iron-and vanadium-doped TiO2 as visible light–sensitive photocatalysts, Constr. Build. Mater. 149 (2017) 257–271, https://doi.org/10.1016/j.conbuildmat.2017.05.132.
[29] S.S. Lucas, V.M. Ferreira, J.B. De Aguiar, Incorporation of titanium dioxide nanoparticles in mortars—Influence of microstructure in the hardened state properties and photocatalytic activity, Cem. Concr. Res. 43 (2013) 112–120, https://doi.org/10.1016/j.cemconres.2012.09.007.
[30] C. Giosuè, Q.L. Yu, M.L. Ruello, F. Tittarelli, H.J.H. Brouwers, Effect of pore structure on the performance of photocatalytic lightweight lime-based finishing mortar, Constr. Build. Mater. 171 (2018) 232–242, https://doi.org/10.1016/j.conbuildmat.2018.03.106.
[31] R. Sugrañez, J.I. Álvarez, M. Cruz-Yusta, I. Mármol, J. Morales, J. Vila, L. Sánchez, Enhanced photocatalytic degradation of NOx gases by regulating the microstructure of mortar cement modified with titanium dioxide, Build. Environ. 69 (2013) 55–63, https://doi.org/10.1016/j.buildenv.2013.07.014.
[32] J. Chen, C.S. Poon, Photocatalytic activity of titanium dioxide modified concrete materials–Influence of utilizing recycled glass cullets as aggregates, J. Environ. Manage. 90 (11) (2009) 3436–3442, https://doi.org/10.1016/j.jenvman.2009.05.029.
[33] C.S. Poon, E. Cheung, NO removal efficiency of photocatalytic paving blocks prepared with recycled materials, Constr. Build. Mater. 21 (8) (2007) 1746–1753, https://doi.org/10.1016/j.conbuildmat.2006.05.018.
[34] V. Matějka, P. Matějková, P. Kovář, J. Vlček, J. Přikryl, P. Červenka, Z. Lacný, J. Kukutschová, Metakaolinite/TiO2 composite: Photoactive admixture for building materials based on Portland cement binder, Constr. Build. Mater. 35 (2012) 38–44, https://doi.org/10.1016/j.conbuildmat.2012.02.086.
[35] B.Y. Lee, A.R. Jayapalan, M.H. Bergin, K.E. Kurtis, Photocatalytic cement exposed to nitrogen oxides: Effect of oxidation and binding, Cem. Concr. Res. 60 (2014) 30–36, https://doi.org/10.1016/j.cemconres.2014.03.003.
[36] M.Z. Guo, A. Maury-Ramirez, C.S. Poon, Photocatalytic activities of titanium dioxide incorporated architectural mortars: Effects of weathering and activation light, Build. Environ. 94 (2015) 395–402, https://doi.org/10.1016/j.buildenv.2015.08.027.
[37] M. Xu, Y. Bao, K. Wu, T. Xia, H.L. Clack, H. Shi, V.C. Li, Influence of TiO2 incorporation methods on NOx abatement in Engineered Cementitious Composites, Constr. Build. Mater. 221 (2019) 375–383, https://doi.org/10.1016/j.conbuildmat.2019.06.053.
[38] M. Xu, H. Clack, T. Xia, Y.i. Bao, K. Wu, H. Shi, V. Li, Effect of TiO2 and fly ash on photocatalytic NOx abatement of engineered cementitious composites, Constr. Build. Mater. 236 (2020) 117559, https://doi.org/10.1016/j.conbuildmat.2019.117559.
[39] E. Boonen, A. Beeldens, Recent photocatalytic applications for air purification in Belgium, Coatings. 4 (3) (2014) 553–573, https://doi.org/10.3390/coatings4030553.
[40] X.F. Chen, S.C. Kou, C.S. Poon, Rheological behaviour, mechanical performance, and NOx removal of photocatalytic mortar with combined clay brick sands-based and recycled glass-based nano-TiO2 composite photocatalysts, Constr. Build. Mater. 240 (2020), 117698, https://doi.org/10.1016/j.conbuildmat.2019.117698.
[41] Q. Jin, E.M. Saad, W. Zhang, Y. Tang, K.E. Kurtis, Quantification of NOx uptake in plain and TiO2-doped cementitious materials, Cem. Concr. Res. 122 (2019) 251–256, https://doi.org/10.1016/j.cemconres.2019.05.010.
[42] R. Feret, Sur la compacité des mortiers hydrauliques, Annales des Ponts et Chaussees 4 (1892) 5–16.
[43] W.B. Fuller, S.E. Thompson, The laws of proportioning concrete, Trans. Am. Soc. Civil Eng. 33 (1907) 222–298.
[44] J. Funk, D. Dinger, J.E. Funk Jr., Coal Grinding and Particle Size Distribution Studies for Coal-Water Slurries at High Solids Content, Final Report, Empire State Electric Energy Research Corporation, New York, (1980).
[45] A.H.M. Andreasen, J. Andersen, Über die Beziehung zwischen Kornabstufung und Zwischenraum in Produkten aus losen Körnern (mit einigen Experimenten), Colloid Polym. Sci. 50 (3) (1930) 217–228.
[46] V. Johansen, P.J. Andersen, Particle Packing and Concrete Properties, in: J. Skalny, S. Mindess (Eds.), Materials Science of Concrete II, The American Ceramic Society, Westerville, OH, 1991.
[47] Ö. Sevim, İ. Demir, Optimization of fly ash particle size distribution for cementitious systems with high compactness, Constr. Build. Mater. 195 (2019) 104–114, https://doi.org/10.1016/j.conbuildmat.2018.11.080.
[48] Ö. Sevim, İ. Demir, Physical and permeability properties of cementitious mortars having fly ash with optimized particle size distribution, Cem. Concr. Compos. 96 (2019) 266–273, https://doi.org/10.1016/j.cemconcomp.2018.11.017.
[49] J.L. Lim, S.N. Raman, M. Safiuddin, M.F.M. Zain, R. Hamid, Autogenous shrinkage, microstructure, and strength of ultra-high performance concrete incorporating carbon nanofibers, Mater. 12 (2) (2019) 320, https://doi.org/10.3390/ma12020320.
[50] ASTM C494 / C494M-19, Standard Specification for Chemical Admixtures for Concrete, ASTM International, West Conshohocken, PA, 2019, www.astm.org 10.1520/C0494_C0494M-19.
[51] O. Şahin, S. Bay, H. İlcan, G. Yıldırım, M. Şahmaran, Influence of mixing methods on the NO reduction capability and electrical properties of photocatalytic cementitious systems, Cem. Concr. Compos. 115 (2021), 103840, https://doi.org/10.1016/j.cemconcomp.2020.103840.
[52] L. Cassar, A. Beeldens, N. Pimpinelli, G. L. Guerrini, Photocatalysis of cementitious materials. In International RILEM Symposium on Photocatalysis, Environ. Constr. Mater. 1 (2007) 131-145.
[53] H. Dylla, M.M. Hassan, L.N. Mohammad, T. Rupnow, E. Wright, Evaluation of environmental effectiveness of titanium dioxide photocatalyst coating for concrete pavement, Transp. Res. Rec. 2164 (1) (2010) 46–51, https://doi.org/10.3141/2164-06.
[54] J. Balbuena, M. Cruz-Yusta, A. Pastor, L. Sánchez, α-Fe2O3/SiO2 composites for the enhanced photocatalytic NO oxidation, J. Alloys Compd. 735 (2018) 1553–1561, https://doi.org/10.1016/j.jallcom.2017.11.259.
[55] H. Si, M. Zhou, Y. Fang, J. He, L.u. Yang, F. Wang, Photocatalytic concrete for NOx degradation: Influence factors and durability, Constr. Build. Mater. 298 (2021) 123835, https://doi.org/10.1016/j.conbuildmat.2021.123835.
[56] E. Mohseni, B.M. Miyandehi, J. Yang, M.A. Yazdi, Single and combined effects of nano-SiO_2, nano-Al_2O and nano-TiO_2 on the mechanical, rheological and durability properties of self-compacting mortar containing fly ash, Constr. Build. Mater. 84 (2015) 331–340, https://doi.org/10.1016/j.conbuildmat.2015.03.006.
[57] Z. Li, B. Han, X. Yu, S. Dong, L. Zhang, X. Dong, J. Ou, Effect of nano-titanium dioxide on mechanical and electrical properties and microstructure of reactive powder concrete, Mater. Res. Express 4 (9) (2017), 095008, https://doi.org/10.1088/2053-1591/aa87db.
[58] J. Chen, S.C. Kou, C.S. Poon, Hydration and properties of nano-TiO_2 blended cement composites, Cem. Concr. Compos. 34 (5) (2012) 642–649, https://doi.org/10.1016/j.cemconcomp.2012.02.009.
[59] B. Han, L. Zhang, S. Zeng, S. Dong, X. Yu, R. Yang, J. Ou, Nano-core effect in nano-engineered cementitious composites, Compos. Part A: Appl. Sci. Manuf. 95 (2017) 100–109, https://doi.org/10.1016/j.compositesa.2017.01.008.
[60] H.F.W. Taylor, Cement Chemistry, 2nd edition, Thomas Telford, London, 1997.
[61] T. Chernet, Effect of Mineralogy and Texture in the TiO2 Pigment Production Process of the Tellnes Ilmenite Concentrate, Mineral. Petrol. 67 (1999) 21–32.
[62] B.Y. Lee, K.E. Kurtis, Influence of TiO2 nanoparticles on early C3S hydration, J. Am. Ceram. Soc. 93 (10) (2010) 3399–3405, https://doi.org/10.1111/j.1551-2916.2010.03868.x.
[63] P.C. Aitcin, R.J. Flatt, Science and technology of concrete admixtures, in Woodhead Publishing series in civil and structural engineering number 59, Woodhead Publishing is an Imprint of Elsevier, Cambridge, UK, 2016.
[64] T.K. Erdem, S. Demirhan, G. Yıldırım, Q.S. Banyhussan, O. Şahin, M.H. Balav, M. Şahmaran, Effects of Mixture Design Parameters on the Mechanical Behavior of High-Performance Fiber-Reinforced Concretes, J. Mater. Civil Eng. 32 (12) (2020) 04020368, https://doi.org/10.1061/(ASCE)MT.1943-5533.0003459.
[65] M. Xu, Y. Bao, K. Wu, H. Shi, X. Guo, V.C. Li, Multiscale investigation of tensile properties of a TiO_2-doped Engineered Cementitious Composite, Constr. Build. Mater. 209 (2019) 485–491, https://doi.org/10.1016/j.conbuildmat.2019.03.112.

[66] E. Jimenez-Relinque, J.R. Rodriguez-Garcia, A. Castillo, M. Castellote, Characteristics and efficiency of photocatalytic cementitious materials: Type of binder, roughness and microstructure, Cem. Concr. Res. 71 (2015) 124–131, https://doi.org/10.1016/j.cemconres.2015.02.003.
[67] A.R. Jayapalan, B.Y. Lee, K.E. Kurtis, Can nanotechnology be 'green'? Comparing efficacy of nano and microparticles in cementitious materials, Cem. Concr. Compos. 36 (2013) 16–24, https://doi.org/10.1016/j.cemconcomp.2012.11.002.
[68] A. Al-Dahawi, O. Öztürk, F. Emami, G. Yıldırım, M. Şahmaran, Effect of mixing methods on the electrical properties of cementitious composites incorporating different carbon-based materials, Constr. Build. Mater. 104 (2016) 160–168, https://doi.org/10.1016/j.conbuildmat.2015.12.072.
[69] S. Yeşilmen, Y. Al-Najjar, M.H. Balav, M. Şahmaran, G. Yıldırım, M. Lachemi, Nano-modification to improve the ductility of cementitious composites, Cem. Concr. Res. 76 (2015) 170–179, https://doi.org/10.1016/j.cemconres.2015.05.026.
[70] Y. Al-Najjar, S. Yeşilmen, A. M. Al-Dahawi, M. Şahmaran, G. Yıldırım, M. Lachemi, L. Amleh, Physical and chemical actions of nano-mineral additives on properties of high-volume fly ash engineered cementitious composites, ACI Mater. J. 113(6) (2016) 791-801. 10.14359/51689114.
[71] S. Kawashima, J.W.T. Seo, D. Corr, M.C. Hersam, S.P. Shah, Dispersion of CaCO3 nanoparticles by sonication and surfactant treatment for application in fly ash–cement systems, Mater. Struct. 47 (6) (2014) 1011–1023, https://doi.org/10.1617/s11527-013-0110-9.
[72] C.B. Almquist, P. Biswas, Role of Synthesis Method and Particle Size of Nanostructured TiO_2 on Its Photoactivity, J. Catal. 212 (2) (2002) 145–156, https://doi.org/10.1006/jcat.2002.3783.
[73] C. Minero, F. Catozzo, E. Pelizzetti, Role of adsorption in photocatalyzed reactions of organic molecules in aqueous titania suspensions, Langmuir. 8 (2) (1992) 481–486.
[74] M. Lackhoff, X. Prieto, N. Nestle, F. Dehn, R. Niessner, Photocatalytic activity of semiconductor-modified cement-influence of semiconductor type and cement ageing, Appl. Catal. B: Environ. 43 (3) (2003) 205–216, https://doi.org/10.1016/S0926-3373(02)00303-X.
[75] A. Mills, S. Elouali, The nitric oxide ISO photocatalytic reactor system: measurement of NO removal activity and capacity, J. of Photochem. Photobiol. A: Chem. 305 (2015) 29–36, https://doi.org/10.1016/j.jphotochem.2015.03.002.
[76] H. Wang, Z. Wu, W. Zhao, B. Guan, Photocatalytic oxidation of nitrogen oxides using TiO2 loading on woven glass fabric, Chemosphere 66 (1) (2007) 185–190, https://doi.org/10.1016/j.chemosphere.2006.04.071.
[77] R. Han, R. Andrews, C. O'Rourke, S. Hodgen, A. Mills, Photocatalytic air purification: Effect of HNO3 accumulation on NOx and VOC removal, Catalysis Today. 380 (2021) 105–113, https://doi.org/10.1016/j.cattod.2021.04.017.
[78] L. Yang, A. Hakki, F. Wang, D.E. Macphee, Photocatalyst efficiencies in concrete technology: The effect of photocatalyst placement, Appl. Catal. B: Environ. 222 (2018) 200–208, https://doi.org/10.1016/j.apcatb.2017.10.013.
[79] F IUPAC. (1971). Manual of symbols and terminology for physicochemical quantities and units. Appendix II: definitions, terminology and symbols in colloid and surface chemistry. Everett DH, editor.
[80] L. Jones, Interference mechanisms in waste stabilization/solidification processes, J. Hazard. Mater. 24 (1) (1990) 83–88, https://doi.org/10.1016/0304-3894(90)80005-O.
[81] P.K. Mehta, P.J.M. Monteiro, Concrete Structure, Properties and Materials vol. 2 (1993) 548.
[82] H.W. Song, S.J. Kwon, Permeability characteristics of carbonated concrete considering capillary pore structure, Cem. Concr. Res. 37 (6) (2007) 909–915, https://doi.org/10.1016/j.cemconres.2007.03.011.
[83] V. Cirkva, H. Žabová, Thin nanoporous titania films on the electrodeless discharge lamps for photocatalysis, Preparation, Structure and Applications, Handbook of Photocatalysts, 2010.
[84] X. Wang, K. Wang, J. Tanesi, A. Ardani, Effects of nanomaterials on the hydration kinetics and rheology of Portland cement pastes, Adv. Civil Eng. Mater. 3 (2) (2014) 142–159, https://doi.org/10.1520/ACEM20140021.
[85] L. Znaidi, R. Seraphimova, J.F. Bocquet, C. Colbeau-Justin, C. Pommier, A semi-continuous process for the synthesis of nanosize TiO_2 powders and their use as photocatalysts, Mater. Res. Bull. 36 (5–6) (2001) 811–825, https://doi.org/10.1016/S0025-5408(00)00482-7.